



Cite this: DOI: 10.1039/c8tc05014g

Physical vapour deposition of vanadium dioxide for thermochromic smart window applications

Tuan Duc Vu,^{†^{a,b}} Zhang Chen,^{†^c} Xianting Zeng,^b Meng Jiang,^d Shiyu Liu,^{*^b} Yanfeng Gao  ^{*^{ce}} and Yi Long  ^{*^{af}}

Smart windows are defined by their ability to regulate incoming solar radiation in order to reduce the energy consumption of buildings by modulating the heat intake. Vanadium dioxide (VO_2) is one of the most promising potential candidates for smart window materials due to its ability to reversibly transit from monoclinic VO_2 (M) to rutile VO_2 (R) at near room temperature. As a result of this transition, the infrared radiation (IR) transparent VO_2 (M) abruptly becomes IR opaque, effectively regulating the heat intake by solar radiation. Despite their promising potential, VO_2 -based smart windows have various significant intrinsic limitations: a high transition temperature (τ_c) of 68 °C; low luminous transmission (T_{lum}) of around 40% and low solar modulation (ΔT_{sol}) of less than 25%. Currently, various methods have been used to fabricate VO_2 thin films in an attempt to improve their intrinsic properties. One of those methods is physical vapour deposition (PVD). In this paper, various PVD techniques, such as pulsed laser deposition (PLD), evaporation decomposition (ED) and sputtering, are examined with respect to their conditions for VO_2 fabrication, film quality and the strategies for film improvements. Lastly, some challenges and opportunities for further studies into VO_2 -based smart windows are discussed.

Received 4th October 2018,
Accepted 19th December 2018

DOI: 10.1039/c8tc05014g

rsc.li/materials-c

1. Introduction

As the world population is reaching ever closer to 8 billion people, the global energy demand is also increasing rapidly to accommodate this number. It is estimated that by 2020, the total energy demand will be up to 80% higher than that in 1990.¹ It is clearly crucial to reduce the energy demand by adopting energy conservation strategies. The energy consumption of the buildings sector, both residential and commercial, now exceeds the contributions from the transport and industrial sectors and has climbed to a staggering 40% of the total energy consumption in the last decade.² Within building services, up to 50% of the energy is consumed by heating, ventilation and air conditioning applications (HVAC).³ Following this line of thought, conserving

energy usage for HVAC applications is a logical step in order to reduce the overall energy consumption. Several methods have been proposed to follow this direction including but not limited to: adding insulation materials to walls,⁴ using cool coatings on roofs⁵ and utilizing smart window coatings.⁶

As one of the main gateways to conducting heat between the inner and outer environment, windows are typically energy inefficient due to an undesirable heat exchange, with heat accumulation during summer and heat leakage during winter.^{7,8} Thus, smart windows have received significant attention from both the industrial and academic sectors in recent years. Smart windows are defined by their ability to regulate the transmittance of a certain portion of the solar radiation spectra, which consists of ultraviolet (UV), visible and infrared (IR) radiation. Various materials with different radiation-regulating mechanisms have been studied, namely photochromic, electrochromic and thermochromic. One such material is vanadium dioxide (VO_2), a thermochromic material with metal-insulator transition (MIT) at near room temperature.⁹ Below its transition temperature (τ_c), VO_2 has a monoclinic structure and is transparent to near-IR. Upon reaching above its τ_c , VO_2 adopts a rutile structure, and becomes metallic and opaque to near-IR.¹⁰ Based on its properties, VO_2 is attractive as a smart window material because of a couple of simple reasons: (1) its modulating ability only affects the near IR and does not affect the visible spectrum, thus effectively controlling heat intake by solar radiation while minimizing the energy needed for illumination; (2) no external energy is required to

^a School of Materials Science and Engineering, Nanyang Technological University, 50 Nanyang Avenue, Singapore 639798, Singapore. E-mail: longyi@ntu.edu.sg

^b Singapore Institute of Manufacturing Technology (SIMTech), 2 Fusionopolis Way, #08-04 Innovis, Singapore 138634, Singapore

^c School of Materials Science and Engineering, Shanghai University, Shanghai 200444, China

^d College of Medical Imaging, Shanghai University of Medicine and Health Sciences, Shanghai, 201318, China

^e School of Materials Science and Energy Engineering, Foshan University, Foshan 528000, China

^f Singapore-HUJ Alliance for Research and Enterprise (SHARE), Nanomaterials for Energy and Energy-Water Nexus (NEW), Campus for Research Excellence and Technological Enterprise (CREATE), Singapore 138602, Singapore

† These authors contributed equally.

activate the modulation, as the response is spontaneous when the environment temperature reaches τ_c .^{11,12} However, VO₂ has not yet been commercialized widely due to some intrinsic limitations. First, the τ_c of bulk VO₂ (M) is at about 68 °C, which is too high for practical usage. At the same time, VO₂ has low solar modulation (ΔT_{sol}) and luminous transmittance (T_{lum}). The theoretical predicted ΔT_{sol} of VO₂ is 25% with a moderate T_{lum} of about 40%,¹³ while the typical experimental results indicate ΔT_{sol} at less than 20% and T_{lum} at approximately 40%.¹⁴

In a quest to improve the optical properties of VO₂ and to lower its τ_c , various fabrication methods have been used, including but not limited to chemical vapour deposition (CVD),¹⁵ hydro-thermal,^{16–18} sol-gel synthesis^{19–21} and physical vapour deposition (PVD). PVD refers to a variety of vacuum deposition methods used to deposit thin films *via* the condensation of a vaporised form of the desired film material onto various substrates. The coating methods involve purely physical processes, such as high-temperature vacuum evaporation with subsequent condensation or plasma sputter bombardment. In the case of VO₂ (M/R) thin films fabrication, pure vanadium, V₂O₃, VO₂ or V₂O₅ is commonly used as the target. The partial pressure of oxygen in the deposition chamber is accurately controlled to prevent the formation of other vanadium oxides with different valences, and the substrates are heated to relatively high temperatures to promote the crystallisation of VO₂ (M/R). Compared with other techniques, PVD can achieve high film uniformity, good adhesion and a high packing density. Furthermore, PVD techniques are suitable for large-scale industrial production, which is crucial for the implementation of VO₂ as a smart window solution.^{22–24} Specifically, some widely used PVD techniques include pulsed laser deposition (PLD), evaporation decomposition (ED) and sputtering. This review aims to understand these techniques of VO₂ thin films fabrication, in terms of the fabricated film quality, process control, target requirements, film structure modification (*i.e.* doping) and process-microstructure-property relationship.

2. Reactive pulse laser deposition (RPLD)

RPLD is a widely used method for VO₂ thin film preparation. During this method, a high-power pulsed laser beam is used to strike the target in vacuum (Fig. 1). Although there are relatively few requirements for suitable targets (available targets include metals, metallic oxides powder and ceramics), the deposition processing is complex. The laser pulse is absorbed by the target and converted to different kinds of energy, including thermal, chemical and mechanical energy. During this process, the target could be evaporated, ablated, ionized and even exfoliated. Moreover, the form of ejected species that are produced by laser include electrons, ions, atoms, molecules, clusters, particulates and molten globules.²⁵ RPLD is a powerful technique that enables the fabrication of high-quality VO₂ thin films by controlling their deposition parameters. Also the co-doping of VO₂ films could be easily achieved by ablating dual targets.

Borek *et al.* were the first researchers to prepare VO₂ (M/R) thin films using PLD.²⁶ They adopted a pulsed excimer laser

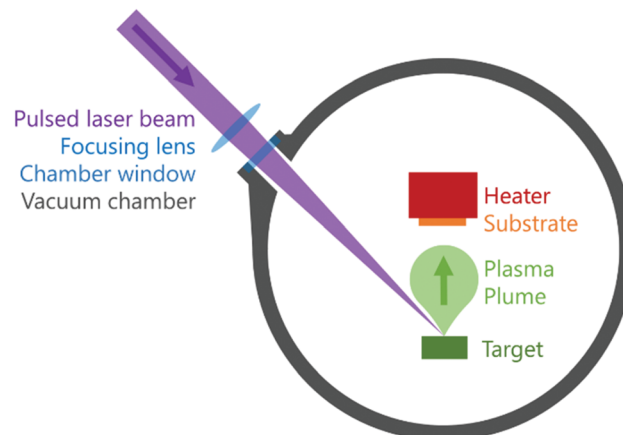


Fig. 1 A typical experimental arrangement for PLD (https://en.wikipedia.org/wiki/Pulsed_laser_deposition).

(at a wavelength of $\lambda = 248$ nm and a pulse duration of $\tau = 15$ ns) to ablate a metallic vanadium target in an ultrahigh-vacuum deposition chamber. The total gas (Ar and O₂) pressure in the system was maintained between 100 and 200 mTorr (about 13–26 Pa). An oxygen concentration of approximately 10% was found to be optimal for the fabrication of pure VO₂ films. Thin films were deposited on R-cut sapphire substrates at temperature ranging from 500 °C to 525 °C. The as-deposited thin films were all stored under the same atmosphere and temperature for approximately 1 h to obtain VO₂ (M/R) polymorphs.

Various PLD processes have been reported ever since then, with various targets being used, including metallic vanadium, V₂O₃, VO₂ and V₂O₅. Besides the most commonly used KrF excimer laser ($\lambda: 248$ nm), ArF ($\lambda: 193$ nm), XeCl ($\lambda: 308$ nm) and Nd-YAG ($\lambda: 532$ nm) excimer laser have also been adopted as the light source. During the deposition, the oxygen partial pressure is usually controlled between 1.3–6.5 Pa by using pure O₂ or an O₂/Ar mixed gas.^{27,28} In most of the works, the substrate is heated to 400–630 °C during the deposition, while in some works, a post-annealing process has been required to obtain high-quality VO₂ thin films.^{29,30}

2.1. Oxygen partial pressure

Oxygen partial pressure is one of the key parameters during VO₂ thin film preparation. An improper oxygen partial pressure could not only lead to the formation of other vanadium oxides, such as V₂O₃,³¹ V₆O₁₃,³² or V₂O₅,³³ but could also influence the morphology and phase transition behaviour of the VO₂ films (Fig. 2a–f).^{34,35} Fan *et al.*³⁶ found that the obtained phases of VO₂ could be controlled by adjusting the oxygen partial pressure during the deposition. That is, a higher oxygen pressure tends to form a VO₂(B) structure, while a lower oxygen pressure favoured VO₂(M1/R) epitaxial growth (Fig. 2g and h). Lafane's work showed that the oxygen pressure influences the process of molecular oxygen dissociation, and resulted in differences in the deposited films' stoichiometric and morphologies.³⁵ There are two important steps: species from the target hit the substrate, leading to re-sputtering, and a shocked layer is formed in

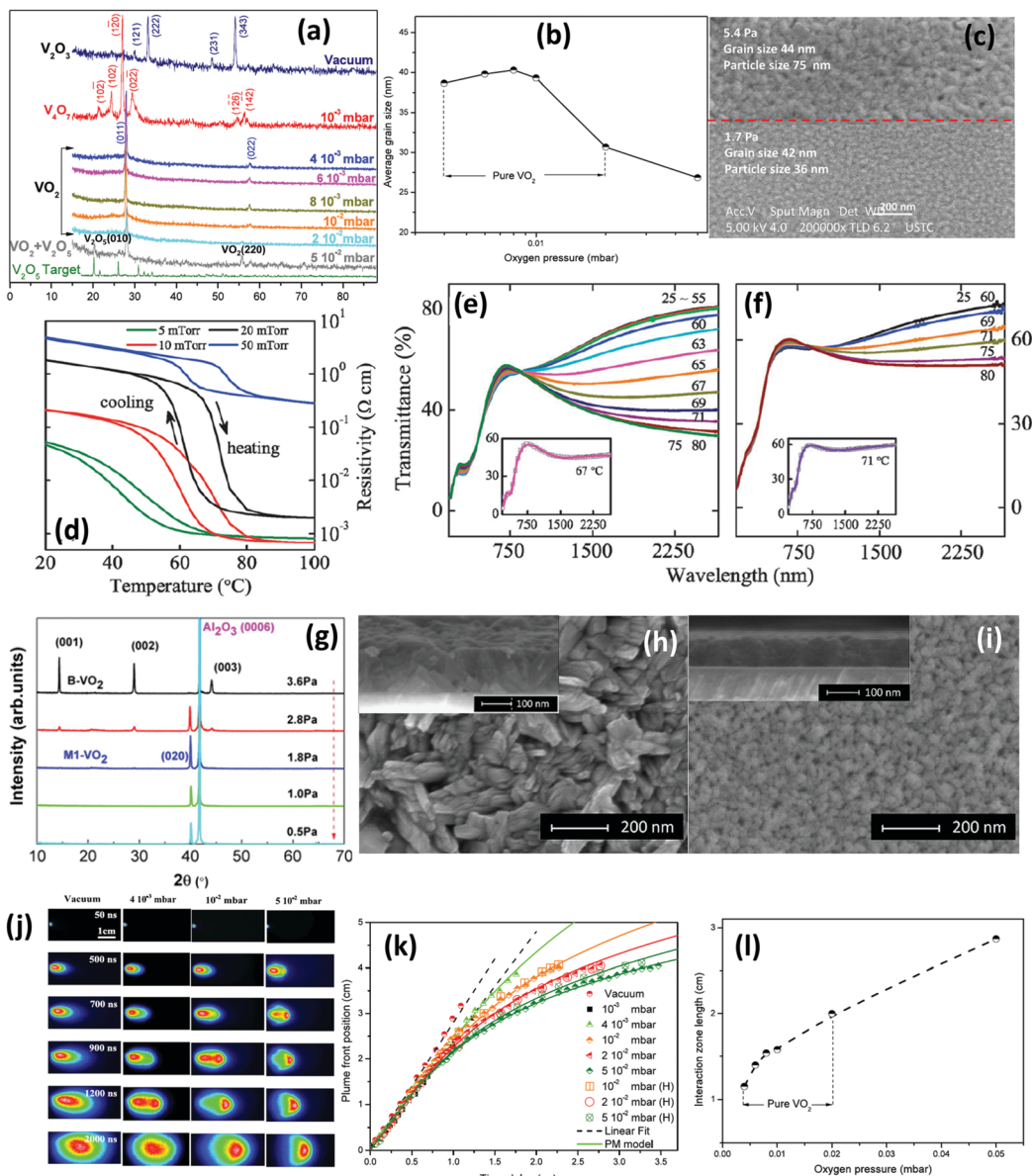


Fig. 2 (a) XRD patterns of the V_2O_5 target and the films and (b) the calculated average grain size deposited at oxygen pressure ranging from 0 to 5×10^{-2} mbar (0 to 5 Pa); (c) surface morphologies of VO_2 thin film prepared at 5.4 Pa and 1.7 Pa; (d) temperature dependence of the electrical resistivity for VO_2 films grown at various oxygen pressures; (e and f) transmittance spectra for VO_2 films grown at 20 and 50 mTorr (2.67 and 6.67 Pa), respectively, inset is the experimental (dotted lines) and best-fitted (solid lines) transmittance spectra of VO_2 films; (g) XRD patterns of VO_2 films deposited on sapphire substrates under different oxygen pressure (0.5–3.6 Pa) with VO_2 target, (h and i) are the surface morphologies of films deposited at 3.6 Pa ($\text{B}-\text{VO}_2$) and 1.8 Pa ($\text{M1}-\text{VO}_2$), and inserts are the related cross-section; (j) temporal evolution of the visible plume under vacuum and at an oxygen pressure of 4×10^{-3} , 10^{-2} and 5×10^{-2} mbar represents the images of the plume obtained during the deposition with the presence of the substrate heater. The position of the ablating surface is at the limit of the left side of the images; (k) plume front position as a function of the time delay at vacuum and different oxygen pressures; (l) distance over which the plume-oxygen gas interaction occurs versus oxygen pressure.

the plume–oxygen gas boundary (Fig. 2j–l), which produces atomic oxygen that could directly be incorporated into the growing film. At a lower oxygen partial pressure, a thin shocked layer forms, while with high velocities of the species hitting the substrate, the strong re-sputtering energies produce homogeneous films, but also favour light elements (O) escaping, forming V_2O_3 , V_4O_7 , etc. At higher oxygen partial pressure, a thick shocked layer forms, offering plenty of atomic oxygen, and the re-sputtering process is weak, so an inhomogeneous film with a stoichiometry

close to the target forms. However, there are other parameters that influence the appearance and performance of the deposited films, albeit the results reported were different in different researchers' work at the same oxygen partial pressure (Fig. 2a and g).

2.2. Substrate temperature

The substrate temperature is another key parameter during RPLD. It is well-known that a higher substrate temperature would favour the formation of high-quality VO_2 (M/R) films. Kim³⁷ prepared

VO_2 films at a substrate temperature as high as 630 °C, where the range of electrical resistance changes (ERC) reached 4×10^5 , comparable to that of single-crystal VO_2 of 10^5 .³⁸ Besides high temperature, Nag *et al.* showed that a post-annealing process after deposition would also help the formation of high-quality samples.²⁹ Samples deposited at room temperature with a following post-annealing process at 450 °C showed obvious advantages in light regulation across the MIT compared to samples deposited at 500 °C without a post-annealing process (Fig. 3). It should be mentioned that the cooling speed would also influence the performance of VO_2 thin films.³⁹

It is an attractive option to prepare VO_2 thin films at a very low substrate temperature. Soltani *et al.*⁴⁰ studied the process of depositing VO_2 films on Kapton substrates using a vanadium target. Although no optical switching was observed in the prepared $\text{VO}_2/\text{Kapton}$ samples, it was discovered that the $\text{VO}_2/\text{Si}(100)$ exhibited the well-known MIT with a transition temperature about 68 °C at deposition temperatures as low as 300 °C. Maaza *et al.*⁴¹ prepared high stoichiometric VO_2 films using a VO_2 target without any substrate heating or atmosphere control. These films could be deposited on silicon, quartz and sapphire substrates. They all showed obvious MIT at ~68 °C with an electrical resistance change of $\sim 10^2$. Liu *et al.*⁴² and Suh *et al.*⁴³ also reported VO_2 films with obvious MIT prepared with a vanadium target on MgO , quartz and n-type silicon substrates. By improving the annealing time, Suh improved the crystalline quality of VO_2 (Fig. 3d), although all these films performed poorly in MIT processing. In recent years, few works on lower temperature deposition can be found, with most studies adopting higher deposition temperatures (500–550 °C).

2.3. Epitaxial growth

Epitaxial growth is one route to obtain high-quality VO_2 . There are several methods to prepare epitaxial VO_2 thin films, such as sputtering,^{44–46} electron beam deposition⁴⁷ and molecular beam epitaxy,^{48,49} while other phases of epitaxy VO_2 could also be prepared, such as $\text{VO}_2(\text{B})$ ⁵⁰ and $\text{VO}_2(\text{A})$ ⁵¹ species produced by pulsed laser are high-energy species, which can assist the *in situ* fabrication of oriented, epitaxial thin films, leading to PLD becoming a more widely used method for the epitaxial growth of VO_2 films.

The first work on VO_2 films prepared by PLD was epitaxial.²⁶ Details of the epitaxial growth of VO_2 thin films can be found in Nag *et al.*'s review²⁵ in 2008. Here, we just focus on the phase transition properties of epitaxial VO_2 films prepared by PLD across MIT, which implies phase transition properties modulation for smart window applications.

Phase-transition properties refer not only to the phase-transition temperature (τ_c), but also to the phase-transition width (ΔH), speed (ΔT) and amplitude (ΔA). ΔH is the difference in the phase transition temperature from the VO_2 (M) to (R) phase and from the VO_2 (R) to (M) phase ($\tau_{\text{C: M-R}} - \tau_{\text{C: R-M}}$), while ΔT is the temperature required for a complete phase transition from the (M) to (R) phase or (R) to (M) phase, and ΔA is the difference in the resistance of transmittance of VO_2 across the MIT. For application in smart windows, the closer τ_c is to room temperature, the narrower the ΔH , the faster the ΔT and the larger the ΔA , the better the energy saving effect the smart window can have.⁵²

For single crystals, the transition widths (ΔH) are less than 0.15 K, and the electrical resistance changes across MIT (ΔA) reaches as large as 5 orders of magnitude, while for un-oriented films,

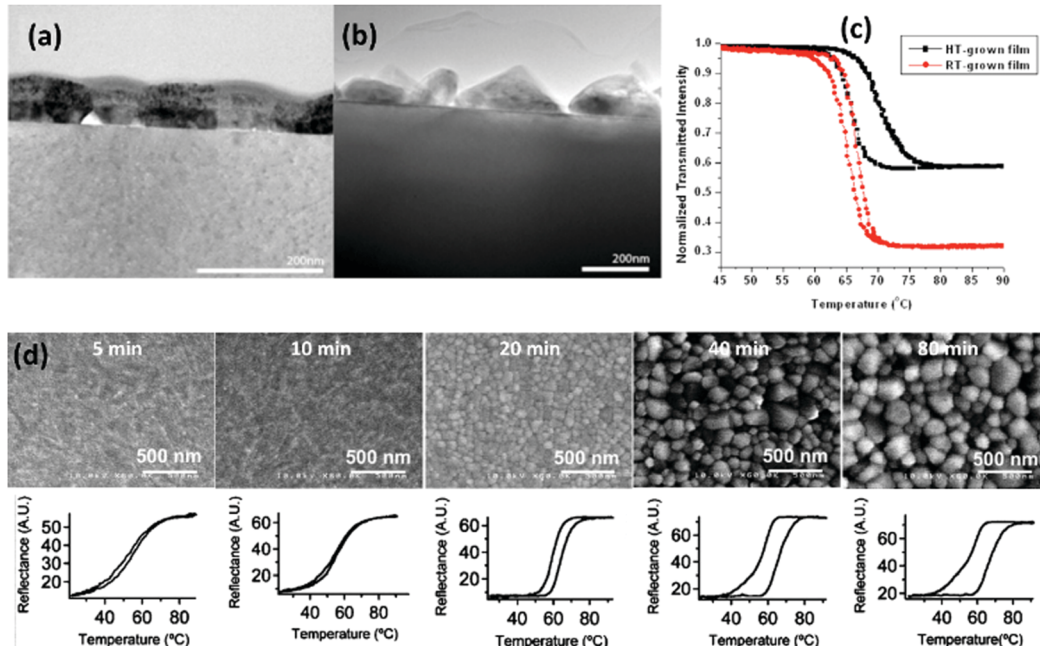


Fig. 3 TEM and light transmission hysteresis for: (a) room temperature deposition followed with 450 °C annealing (RT-grown film) and (b) high temperature deposition at 500 °C (HT-grown film); (c) white light transmission hysteresis for RT grown (red) and HT grown (black) film; (d) SEM and relative IR ($\lambda = 980$ nm) switching curves through the structural phase transition time for 100 nm VO_2 thin film fabricated at 450 °C annealing for 5–80 min in 250 mTorr (~33.3 Pa) of O_2 . As annealing time is increased, hysteresis is enhanced and the sharpness of the transition and grain size are improved.

ΔH ranges from 5 to 40 K,⁵³ and ΔA is usually less than 4 orders of magnitude. For most of the reported epitaxial VO₂ films prepared by PLD, the ΔH could be reduced to as narrow as 2 K, and ΔA is usually larger than 4 orders of magnitude. These indicate the high quality of the oriented VO₂ films. Different from bulk materials, the MIT performance of VO₂ epitaxial films are diverse, mainly caused by the stress in the films. These stresses are induced by a lattice and expansion efficiency mismatch between substrates and films. It has been found that tensile stress along the *c*-axis of a tetragonal unit cell (metal phase) would reduce the MIT temperature, while compressive stress along this direction would improve the MIT temperature,^{54,55} where the thinner the deposited epitaxial VO₂ films, the larger difference in MIT temperature.^{56,57} The MIT temperature of epitaxial VO₂ films could be modified over a wide temperature range (>40 °C).⁵⁴

It was thought that the smaller the mismatch between the substrate and deposited films, the less influence this would have on the MIT performance of VO₂ films. To test this out, oriented VO₂ on different substrates were prepared by PLD, including Al₂O₃ with r-, m- and c-cuts,^{32,58,59} MgO(100)^{32,58} and (111),⁶⁰ MgF₂(001),^{61,62} TiO₂(001),^{63–65} (110),⁶³ (111),⁶⁶ (101)⁶⁶ and (100).⁶⁶ Different MIT performances were obtained due to lattice mismatch (Fig. 4a–d). To modify the stress, a buffer of epitaxial layers of other materials were deposited prior to VO₂, such as TiO₂,^{54,67,68} AlN,⁶⁹ SnO,⁷⁰ Cr₂O₃,⁷¹ and YSZ/NiO.⁷² However, the small misfits required a large distance to relax the misfit strain (critical thickness),⁷³ but as the resistance of dislocation glide in VO₂ is very large, this means the misfits are not able to relax totally.⁵⁴ Although TiO₂(001) had the lowest lattice mismatch with VO₂ (R) (<1%), the MIT temperature of VO₂/TiO₂(001)/Al₂O₃ was much lower than bulk VO₂ (~25 °C)^{54,67,68} (Fig. 4f).

It is possible to achieve high-quality epitaxial VO₂ films with suitable conditions, including substrate materials, orientation, and pre- and post-deposition processes. However, Jian *et al.*'s work (Fig. 4g–k) showed that, due to lattice constant changes and thermal expansions during thermal cycles (17–97 °C), a large strain would accumulate around the domain boundaries in the VO₂ films, resulting in degradations of ΔT and ΔH .⁵⁵ It is thus still a challenge to prepare high-quality VO₂ films with long-term stability for practical usage.

PLD offers advantages in the concise control of the chemical composition, crystallinity and epitaxy growth, and the thinnest VO₂ films with a MIT prepared by PLD is about 2–3 nm,^{56,74} which means the wafer-level fabrication of VO₂ is possible for device applications. However, the PLD method cannot be adopted for VO₂ film growth with a larger size up to one or two inches if considering the film uniformity and the surface defects, which greatly hinders their usage in smart windows and in other applications based on the phase-transition property of the VO₂ material.⁷⁵

3. Ion plating/ion implantation

Ion plating is a method for producing a new phase in a host material by injecting impurities followed by nucleation within

the host. Strictly speaking, ion plating is not a method for thin-film preparation since the nanoparticles prepared by this method are separated by the host material. However, these nanoparticles usually disperse in a very limited depth due to the implanted ion energy (several hundred nanometres), so they effectively act as a thin film, especially in terms of their optical properties. These are called 'nanocomposite' films/coatings in smart window studies. Thin films fabricated by this method perform better than pure VO₂ thin films in luminous transmittance and in their solar energy modulation ability.^{76–78}

A typical ion-plating process for the preparation of VO₂ contains two steps (Fig. 5a): at room temperature, stoichiometric vanadium and oxygen are co-implanted into a substrate, such as SiO₂ or Al₂O₃,⁷⁹ at an energy of about 150–300⁸⁰ (100⁸¹) keV for vanadium and 56–120⁸⁰ (36⁸¹) keV for oxygen, and then the implanted substrate is annealed at a temperature ranging from 700–1000 °C^{82,83} in high-purity flowing argon.

The energy of the ions determine the dispersion depth of the obtained nanoparticles. In Lopez's work, VO₂ nanoparticles of a sample prepared at a vanadium ion power of 300 keV were found within 500 nm of the top surface of the SiO₂ substrate, or within 300 nm when the vanadium ions were at 150 keV. While in Karl's work, the use of a 100 keV vanadium ion source resulted in a particle depth of about 150 nm. Average particle sizes of 30–90 nm could be obtained by changing the annealing time (Fig. 5c). Doping could be easily realized in this method by co-implanting (W,Mo).⁸¹ Moreover, ion implanting could be a general method to perform the non-equilibrium doping of VO₂ films pre-deposited by different methods.^{84,85}

VO₂ nanoparticles prepared by ion implanting are well separated by the matrix, have good crystallinity due to the high annealing temperature and a relatively stable surface (Fig. 5b). These attributes make them ideal samples to study the phase-transition process of VO₂ nanoparticles,^{86–88} even in the case of single-nanoparticle studies.⁸⁹ A particle-size-dependent loop width of VO₂ nanoparticles during phase transition was found and well analyzed through thermodynamics and kinetics studies by Lopez. The phase transition was found to possibly be induced by infrared light pulses of less than 200 fs duration.⁹⁰

The transmittance spectrum of these samples are rarely reported. Instead, the surface plasmon resonance phenomenon of VO₂ nanoparticles at metal phase is better studied.^{90,91} The most obvious difference caused by surface plasmon resonance is a strong absorption in the near-infrared region (mainly at 800–1800 nm). This greatly increases the switching efficiency of VO₂ and is later seen to be one of the greatest advantages of nanocomposite-VO₂-based smart coatings. This helps to promote the usage of VO₂ for smart window application.^{77,92}

However, ion implanting is not a widely used method to prepare VO₂. Compared to other methods, the limitation in substrate selection and the high annealing temperature increase the manufacturing cost and complexity of the process. At the same time, the composite structure of the VO₂ and substrate does not show any advantages over nanocomposite coatings prepared using high-quality VO₂ nanoparticles.⁷⁷ On the contrary, this

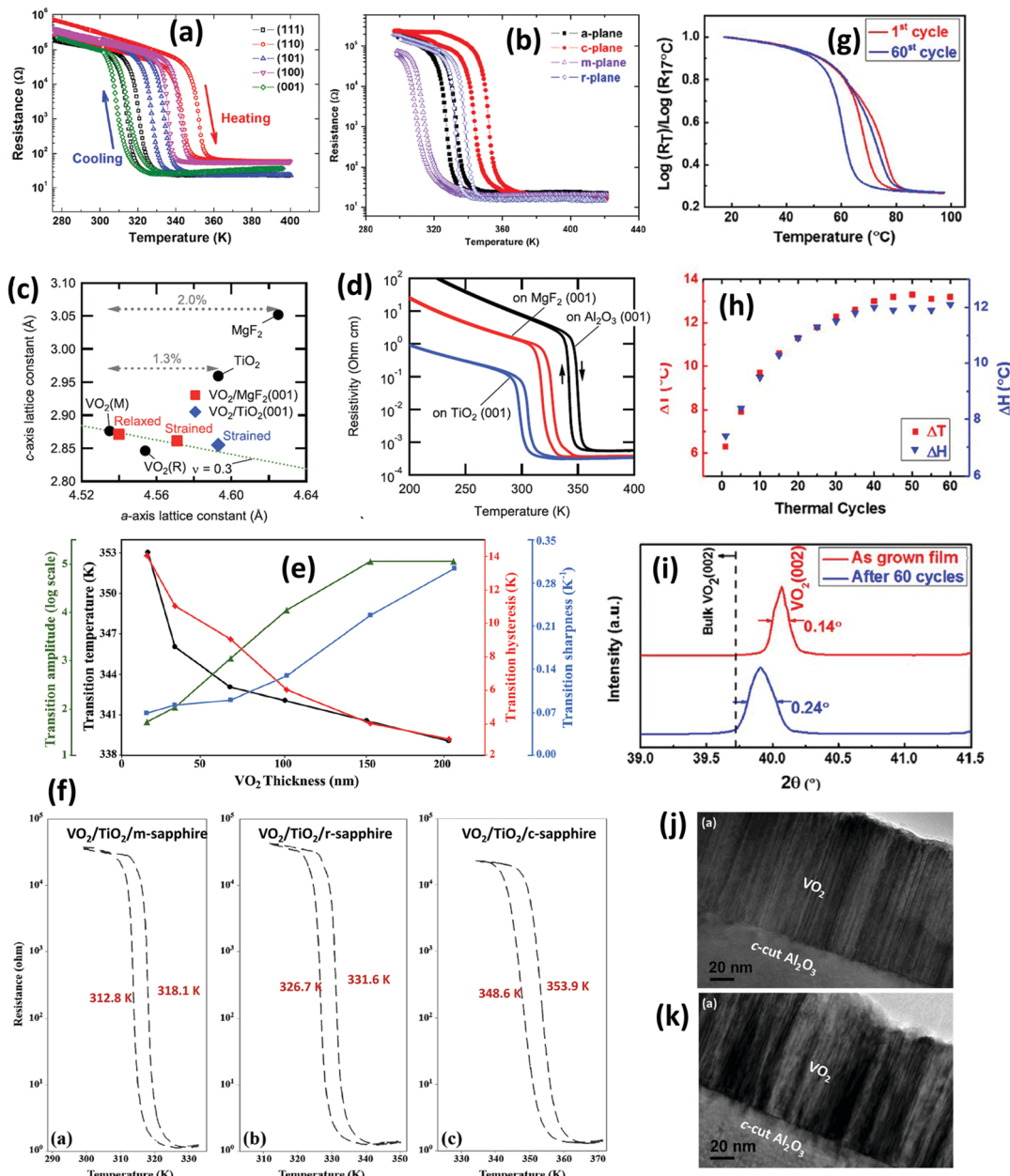


Fig. 4 (a) Temperature-dependent resistance of VO_2 films grown on different orientation TiO_2 substrates and (b) VO_2/TiO_2 bilayers grown on sapphire with different orientations (c-plane, m-plane, r-plane and a-plane); (c) temperature-dependent resistivity of VO_2 thin films deposited on different substrates (TiO_2 , MgF_2 or Al_2O_3) and (d) lattice constants of VO_2 films and TiO_2 , MgF_2 substrates, with lattice constants of the R- and M-phases of VO_2 also plotted, dotted green line is for the strained VO_2 (M) lattice constants; (e) a summary of MIT parameters of VO_2 epitaxial thin films with different thicknesses; (f) temperature-dependent resistance of $\text{VO}_2/\text{TiO}_2/\text{m-sapphire}$, $\text{VO}_2/\text{TiO}_2/\text{r-sapphire}$ and $\text{VO}_2/\text{TiO}_2/\text{c-sapphire}$ heterostructures; (g–k) Jian et al.'s work; (g) temperature-dependent resistance; (h) resistance changing rate and (i) XRD of VO_2 with 1 and 60 cycles of thermal treatment, (j and k) are TEM cross-section images of 1 and 60 cycles of thermal treatment samples, respectively.

structure could limit VO_2 application in areas where good electrical properties is required.

4. Vacuum evaporation

4.1. Thermal evaporation

Thermal evaporation (TE) is also called vacuum evaporation. During this method, the target is thermally evaporated in a

high vacuum chamber, where the vapour condenses on the substrate, forming the thin film. Since there is no interaction between the thermal source (such as laser, plasma and electron beam) with the target, precursors or substrates, the deposition process is simpler compared to other methods (Fig. 6).

A typical process to deposit VO_2 films by TE usually consists of two steps.^{93,94} The first step is to prepare a vanadium-rich metallic film^{93,94} or VO_x film.⁹⁵ The target (typically metallic vanadium,^{94,96} VO_2 ,⁹⁴ V_2O_5 ⁹⁵) is placed in a heated crucible

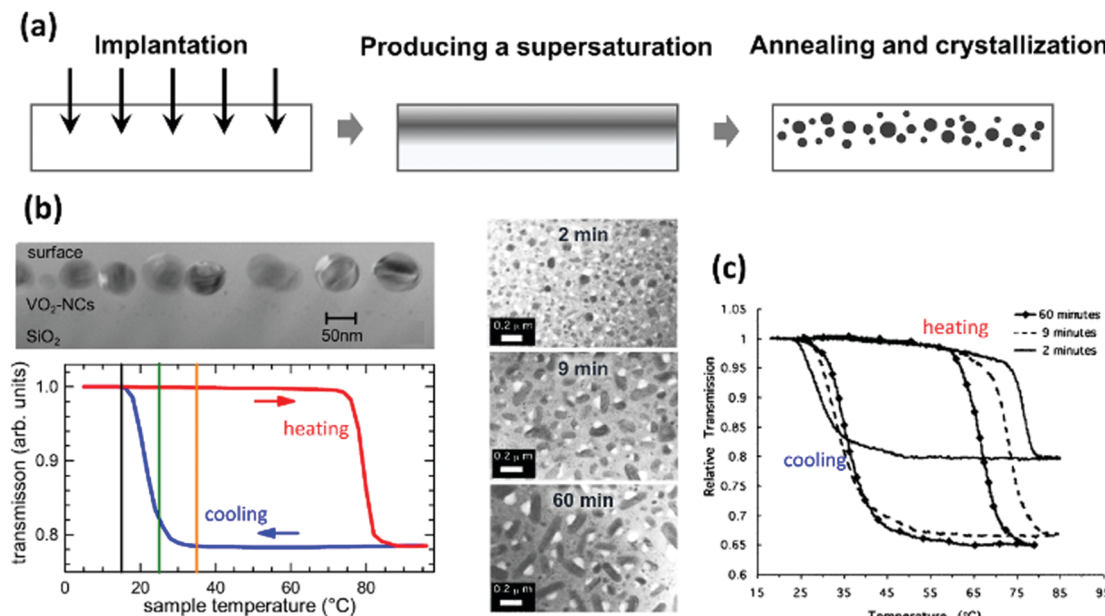


Fig. 5 (a) Schematics of the ion-beam-induced nucleation and ion-implantation process; (b) cross-section TEM image (top) and thermal hysteresis loop of ion-plating-synthesized VO₂ nanocrystals (NCs) in fused silica matrix, with the thermal hysteresis loop obtained by tracking transmission at 1500 nm, and red and blue curves represent the heating and cooling processes, respectively; (c) TEM images (left) and thermal hysteresis loop (right) of VO₂ NCs in fused silica matrix formed at 1000 °C in flowing argon with different annealing times, VO₂ NCs had sizes ranging from dozens to hundreds of nanometres and a size-dependent ΔH as large as 40 °C.

made of Mo or W, located under the substrate in a high vacuum chamber ($2.7\text{--}6.7 \times 10^{-3}$ Pa). Then, the target is resistively heated to evaporate to the substrate, which is pre-heated to 250–300 °C. The as-deposited films required post-annealing at about 400–550 °C under an Ar–O₂ mixed gas⁹⁴ or air (10.7–33.3 Pa)⁹³ to fully convert into VO₂ films. Aside from oxidizing the metallic thin film, Ke *et al.*⁹⁷ reported a method to first grow V₂O₅ nanowires film under atmospheric pressure, then reduced them to VO₂ (R). Other phases, including VO₂ (B) and V₂O₃, could be also obtained by changing the reduction atmosphere.

Jiang *et al.*⁹³ prepared VO₂ films of ~120 nm using TE with a metallic vanadium target. Their films showed a good infrared

control ability (Fig. 7c), which was comparable to films prepared by sputtering. The MIT temperature of these films were less than 60 °C (Fig. 7b). They also found that the MIT performance of the films could be related to the post-annealing time (Fig. 7). The films showed a resistance change of 1 order of magnitude after 2 h annealing and reached to 2 orders of magnitude after 3 h annealing, but would then reduce for longer annealing times. Although TE is simple and promising, the reported works using this method only centred around preparing V₂O₃^{98,99} or VO_x,^{97,100} and few works could be found for VO₂ films preparation after Jiang's work, where it was found that the MIT performance of prepared VO₂ films was weak compared to other methods.^{94,95}

4.2. Electron beam deposition (EBD)

Electron beam deposition is a kind of vacuum evaporation coating method. Different from TE, EBD uses an electron beam to vaporize the evaporation material (Fig. 8). Any material can be evaporated by electron beam evaporation. EBD can be used to prepare multi-component and high-purity films, benefiting from the fact that the electron beam can be accurately controlled and can directly affect the material to be evaporated. EBD equipment is also less expensive than that needed for other physical vapour-deposition techniques and further it shows the potential to produce very smooth films with large size, making it an excellent low-thermal budget deposition method for VO₂ films for optical and electronic applications.¹⁰¹

The EBD of VO₂ requires a basic high-vacuum chamber (below 10^{-4} Pa). A vanadium target is typically used as the evaporation source.^{102–105} The target is put in a crucible under the substrate

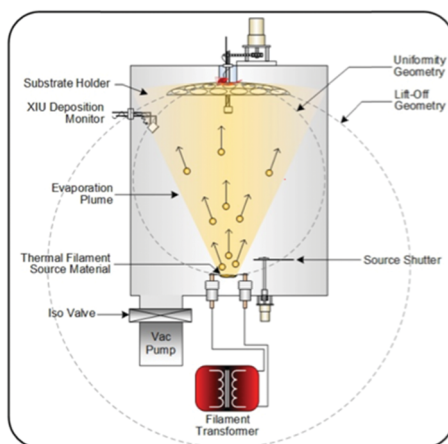


Fig. 6 Diagram of the thermal evaporation process (<http://www.semico.com/news/71-thin-film-deposition-thermal-evaporation>).

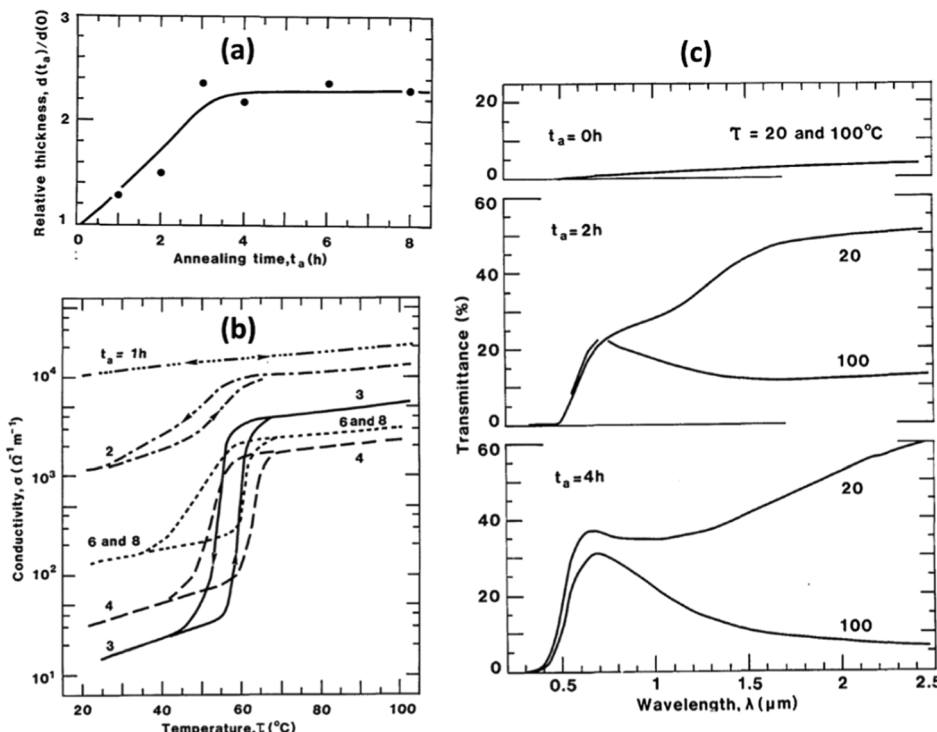


Fig. 7 (a) Relative thickness change with annealing time, indicating the metal vanadium is gradually oxidized to vanadium oxides. Dots represent the measured results and the solid curve the fitted data; (b) temperature dependence of resistance and (c) transmittance curves (250–2500 nm) of samples oxidized with different times. Samples show oblivious resistance and infrared transmittance changes at $\sim 55^\circ\text{C}$ after 2 h oxidization, while ΔA reaches as large as 2 orders of magnitude after 6 h oxidization.

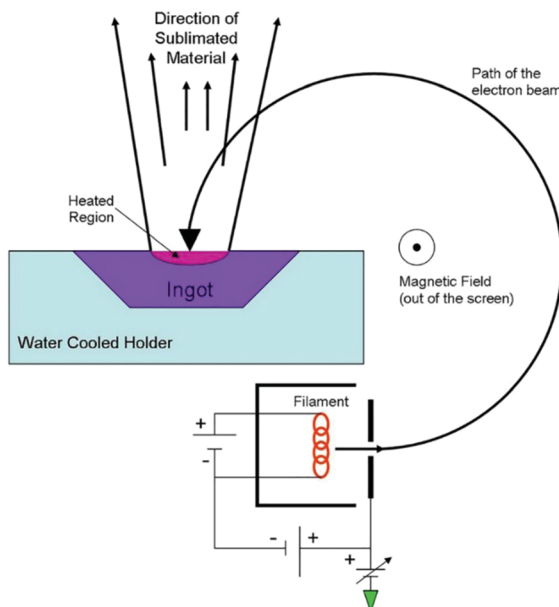


Fig. 8 Diagram of the electron-beam deposition process (https://en.wikipedia.org/wiki/Electron-beam_physical_vapor_deposition).

(about 250 mm). An incident electron beam (accelerating voltage of 10 kV) is used to evaporate the vanadium under a pure oxygen atmosphere (total pressure 0.06–0.1 Pa). The deposition rate of the vanadium oxide films is controlled by a quartz oscillator at

the nominal rate of $0.03\text{--}0.07\text{ nm s}^{-1}$. Doping could be done using doped targets.

VO_2 powder could also be used as an evaporation resource, either in powder form¹⁰¹ or compressed into a sheet.¹⁰⁶ Different from using the vanadium target, oxygen is unnecessary during the evaporation, but a pressure of $\sim 0.5 \times 10^{-4}\text{ Pa}$ is required for pre-treating the VO_2 powder or sheet. System pressure is maintained at $\sim 1.33 \times 10^{-2}\text{ Pa}$ during evaporation. The deposition rate of this method is controlled at about 0.3 nm s^{-1} by quartz crystal microbalance.

It seems that substrate heating during deposition is not the key parameter to obtain high-quality VO_2 films with thermochromic performance, but a post-deposition oxygen annealing step ($450\text{--}550^\circ\text{C}$) or an applied radio frequency (incident power 10–50 W) is. In Marvel *et al.*'s work,¹⁰¹ a post annealing of as short as 5 min at 450°C could generate a pure VO_2 (M) phase from the as-deposited film (Fig. 9a and b). Leroy *et al.*¹⁰³ used radio frequency applied to the substrate to increase the adhesion and decrease the porosity of the forming films during deposition.

Théry *et al.*¹⁰⁵ comprehensively studied films deposited without any treatment (as-grown) with a 50 W radio frequency treatment (discharge) and with post-deposition annealing at 550°C for 15 min (annealed) (Fig. 9c and d). In this work, the as-grown films did not show thermochromic performance even with the substrate heated to 500°C . These films exhibited a poor structural quality (large deviation from stoichiometry, large mosaicity and large strains) and a purely metallic behaviour.

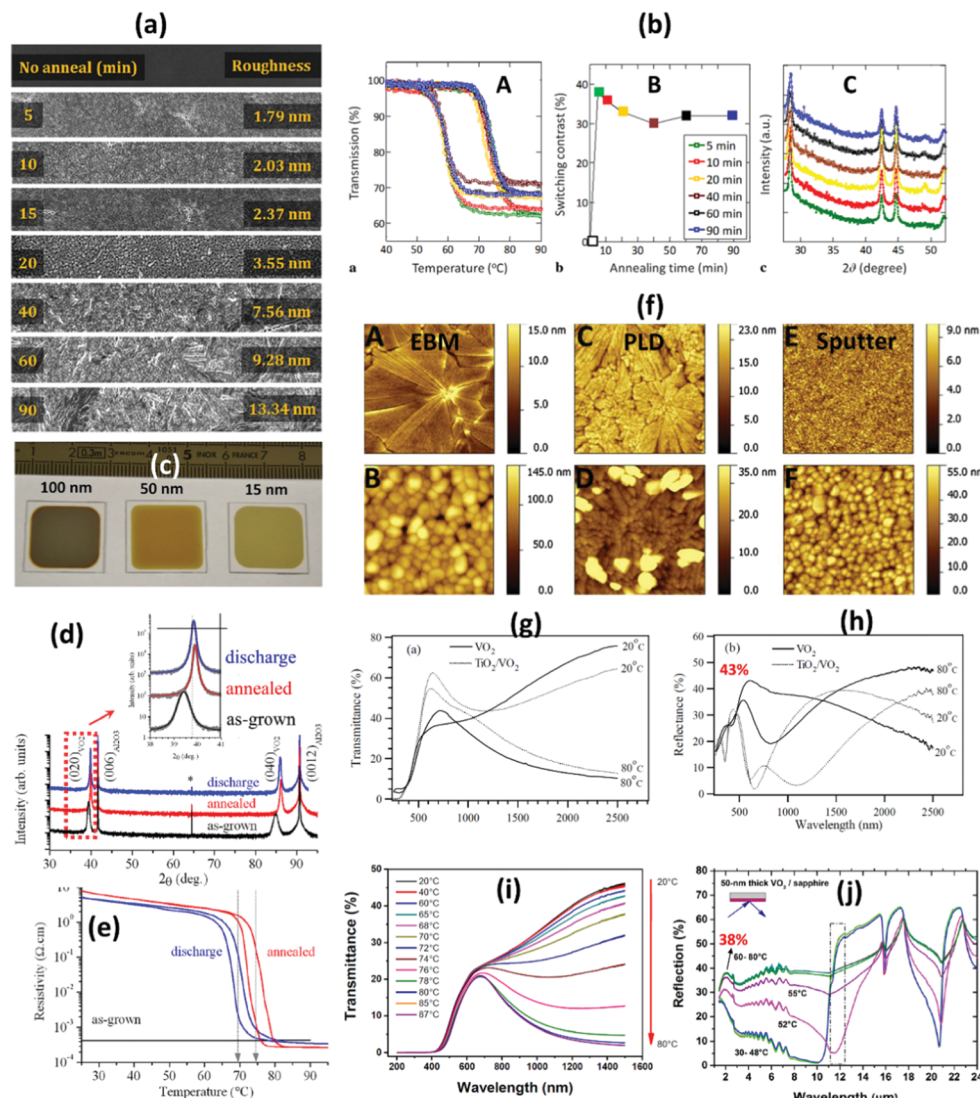


Fig. 9 (a) Surface morphology of an as-grown and annealing (from 5–60 min) VO₂ film prepared by EBD, and their performance (b), (b-A) temperature dependence transmittance, (b-B) switching contrast vs. annealing time and (b-C) XRD; (c) photograph of VO₂ film with different thicknesses prepared by EBD; XRD; (d) temperature dependence of resistance (e) of discharge, annealed and as-grown film, showing the comparable performances of the discharge and annealed films; (f) AFM of VO₂ films prepared by EBD (f-A and f-B), PLD (f-C and f-D) and by sputtering (f-E and f-F); spectra transmittance of VO₂ films prepared by sputtering (g and h) and by EBD (i and j), (g and i) are transmittance at different temperatures, (h) is reflectance from 250–2500 nm, (j) reflectance from 250–25 000 nm.

Meanwhile, the annealed films exhibited an excellent thermochromic performance, with resistivity changes of more than four orders of magnitude across the MIT. These films also exhibited excellent structural properties (a low level of heterogeneous strain, a mosaicity confined into narrow regions close to the interface and a level of strain solely due to the film/substrate thermal expansion mismatch). They also found that films with similar electrical properties could also be obtained by only radio frequency discharge treatment during deposition. Compared to annealed films, these discharge films only suffered slightly degraded structural properties. It is crucial to add radio frequency during the electron-beam deposition of VO₂.

VO₂ films prepared by EBD could reach a comparable performance to that of other physical vapour-deposition techniques.

A resistance change of as high as five orders of magnitude during MIT indicated the fine crystallizability of the obtained VO₂ thin films.¹⁰⁵ Furthermore, uniform films with a size of 100 × 100 mm² were prepared by EBD, which evinced the potential of this method for large-scale preparation.¹⁰⁵ However, Marvel's work showed that the density of films prepared by EBD is slightly lower than that prepared by PLD and by sputtering with similar annealing processing.¹⁰⁷ A similar phenomenon could be inferred from the reflective spectrum of a sample prepared by other researchers,¹⁰² which was seen to be clearly lower than that of the samples prepared by sputtering. The maximum reflectance values were 38% and 43%, respectively, as marked in Fig. 5h and j.¹⁰⁸ The denser the films are, the higher the reflection (Fig. 9g–j). In Marvel's work, the EBD films also

showed lower high-temperature stability, which may be a result of the lower density.¹⁰⁷ A much lower energy of the ejected target material (0.2 eV vs. 50 eV and 10–40 eV of PLD and sputtering, respectively¹⁰⁷) may be one of the reason for the lower density. That is why an applied radio frequency could decrease the porosity of the formed films in Bessaudou's work.¹⁰³ It is clear that the morphological evolution is dominated by strain imparted during the sputtering process. For films deposited by PLD and EBD, the substrate plays a more important role, with substrate de-wetting and epitaxy determining the film structure during solid-phase crystallization.¹⁰⁷

5. Molecular beam epitaxy (MBE)

MBE (Fig. 10) is a widely used method to prepare high quality and homogeneous epitaxial crystal layers. It is highly reproducible in terms of both film thickness and composition control. Although various methods to prepare VO₂ thin films have been studied, a process to prepare VO₂ thin films with a perfect V–O stoichiometry and near single-crystal structure is still very attractive. Studies on the preparation of VO₂ thin films using MBE and their MIT performance could only be found in recent years.

There are two main methods for VO₂ thin films preparation by MBE. The first one, developed by Sambi *et al.*,^{109,110} is called the “periodic annealing” method. Here, before deposition, a TiO₂(110) substrate is cleaned with cycles of Ar-ion sputtering followed by annealing at 573 K in O₂ (1×10^{-6} mbar), to produce sufficient bulk oxygen vacancies to avoid the charging

problem. Then, 0.2–0.5 monolayers (ML), corresponding to 5.2×10^{14} vanadium atoms per cm², of amorphous V metal are deposited in vacuum (5×10^{-11} mbar) at room temperature by electron-beam evaporation. A post annealing process (at 423 K) in an oxygen atmosphere (7.5×10^{-7} – 1.5×10^{-6} mbar) follows to obtain an epitaxial VO₂ layer. The sample is then cooled to room temperature and the next 0.2–0.5 ML of amorphous V metal is deposited. This cycle is repeated until a 3–5 ML thick epitaxial VO₂ layer is obtained.¹¹¹ The films prepared by Sambi showed ordered VO₂ phase grown epitaxially on TiO₂(110) with a rutile-type structure, but no MIT of these films had been observed.

Tashman *et al.*¹¹¹ followed Sambi's work and deposited VO₂ on TiO₂(001). The resulting films did not show MIT either. They developed the following process and alterations:

- (1) Use distilled ozone instead of O₂;
- (2) Increase the temperature from room temperature to 395 K and from 423 K to 473 K for deposition and annealing, respectively;
- (3) Add a rapid post-annealing processing to 673 K (3 K s^{-1} , 1×10^{-6} mbar of distilled ozone).

Detailed parameters are shown in Fig. 11a–c. With these alterations, obvious MIT was observed in films even as thin as 2.3 nm, with a resistance change in orders of magnitude ($\log(\Delta R/R)$) of 1.4. Tashman's work also showed that the transition width decreases monotonically with film thickness, while the hysteresis increases monotonically with film thickness.¹¹¹

Paik *et al.*¹¹² adopted this process for the study of VO₂ thin films (Fig. 11d–j), but with an even higher deposition and annealing temperature (523 K), and a post-annealing process up to 623 K. This annealing step enhances the coalescence of (001)-oriented VO₂ islands, and improves the abruptness of the MIT.¹¹² They also developed a process for TiO₂ substrate pre-treatment.¹¹²

The other method is RF-plasma assisted Oxide Molecular Beam Epitaxy (OMBE), as reported by Fan *et al.*⁷⁵ (Fig. 11k–m). In this method, a standard RF-plasma source was used to provide reactive oxygen radicals. Pure metallic vanadium powder was used as the target for e-beam evaporation. An Al₂O₃ crystal slice or TiO₂ could be used as the substrates, which were degassed and annealed at 823 K in vacuum (4×10^{-9} mbar). The chamber pressure was maintained at $1.3\text{--}4 \times 10^{-5}$ mbar during the film preparation. The evaporation rate of vanadium was controlled at 0.1 A s^{-1} . An optimized flow rate of 1.8 sccm for pure VO₂ film depositions was used as a lower oxygen gas flow would cause oxygen deficiency and could result in V₂O₃ film being formed instead (Fig. 11).

An extremely thin VO₂ film could be prepared by MBE; the thinnest one with MIT reported is 1.5 nm by Paik.¹¹² It seems that the thinner films have a lower MIT temperature.^{111–113} Fan *et al.* studied this phenomenon using interfacial strain dynamics and theoretical calculations, and claimed that the electronic orbital occupancy is strongly affected by the interfacial strain, which also changes the electron–electron correlation and controls the phase-transition temperature.^{113,114} Up to now, the lowest MIT temperature of pure VO₂ thin films reported by MBE was 280.5 K,

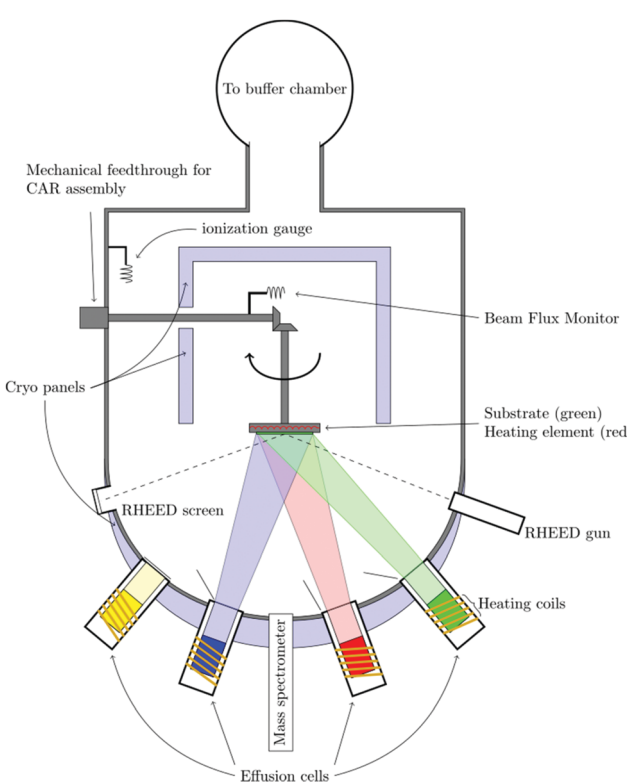


Fig. 10 Simple sketch of a molecular-beam epitaxy system (https://en.wikipedia.org/wiki/Molecular-beam_epitaxy).

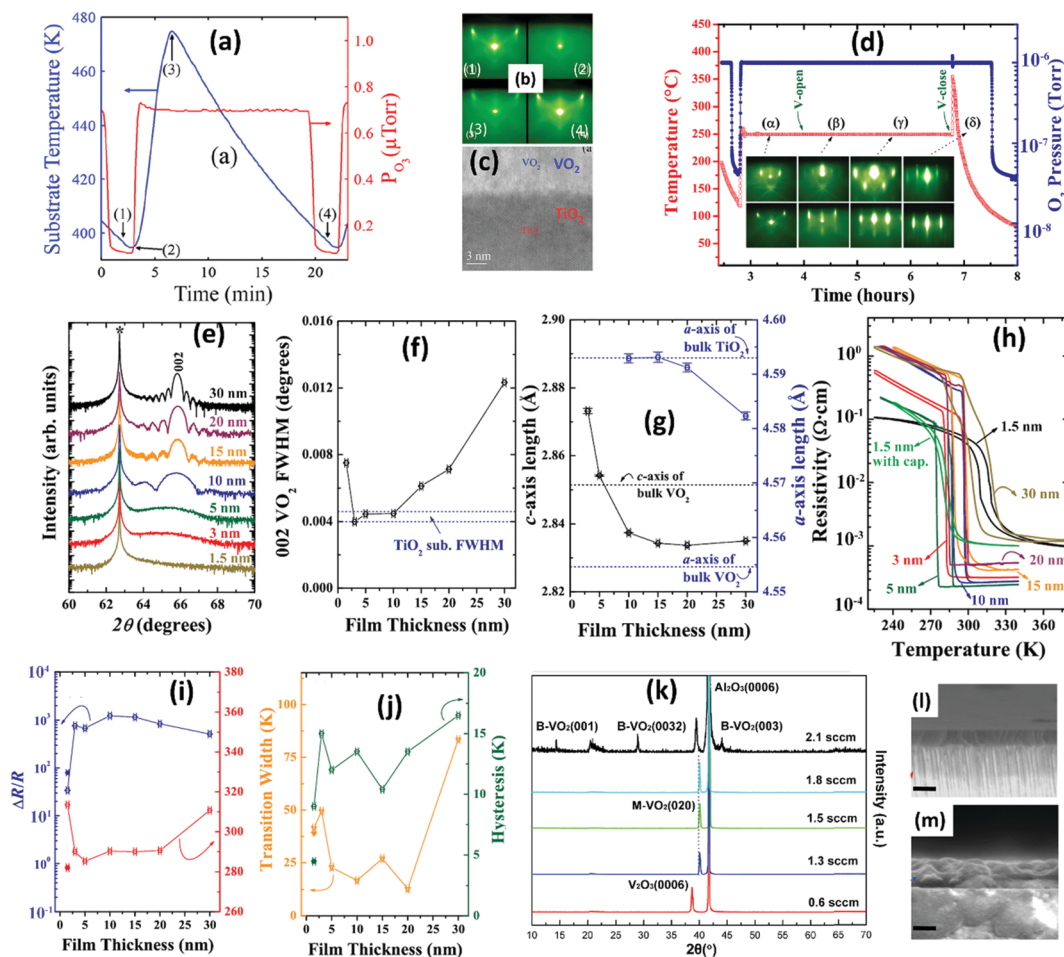


Fig. 11 (a–c), Tashman's work: (a) illustration of the substrate temperature and background pressure of distilled ozone (P_{O_3}) used during the VO_2 growth cycle, (b) RHEED images, along the [100] direction of TiO_2 and VO_2 in the growth cycle. Numbers in (a and b) represent different steps in the growth cycle: (1) prior to vanadium deposition, (2) the time vanadium deposition, (3) post annealing, and (4) the beginning of the next cycle, (c) LAADF-STEM image of the epitaxial VO_2 film; (d–j) work of Paik *et al.*, (d) RHEED patterns observed during the growth of a 10 nm epitaxial VO_2 thin film, (e–j) XRD pattern, FWHM, c -axis length, temperature dependence of resistance, resistance change and transition width of deposited VO_2 films with different thicknesses, respectively; (k–m) work of Fan *et al.*, (k) XRD of VO_2 films prepared at different oxygen flux rates, (l and m) SEM cross-section images of the obtained V_2O_3 and VO_2 .

in which a film thickness of 3.3 nm has resistance changes of 2.3 orders of magnitude. The thinnest film (1.6 nm) did not show the lowest MIT temperature, probably due to diffusion of Ti substrate into the thin film layers.¹¹² However, compared with the epitaxial VO_2 films prepared by PLD on the similar $TiO_2(001)$ substrate with a similar thickness (from 3–15 nm),⁶⁵ these thin epitaxial VO_2 films show lower MIT temperature and smaller resistance changes during MIT. This may indicate higher stresses in these epitaxial VO_2 thin films. More work could still be done in the MIT investigation of MBE epitaxial VO_2 .

Besides the advantages in preparing extremely thin films, MBE also shows advantages in the preparation of large size thin films, accurate stoichiometry, and especially low-temperature deposition (350 °C¹¹¹). Low-temperature deposition for VO_2 means a reduced lattice mismatch due to the thermal expansion and diffusion of substrate elements and higher crystal quality, which can be used in basic theory research^{113,114} and in the development of precision components.^{115,116} It could also enable

the application of VO_2 in electronic devices, such as in uncooled infrared focal plane arrays. However, MBE requires a crystallized substrate with very little lattice mismatch with the deposition materials and expensive equipment, which limit its wide usage.

6. Sputtering

Sputtering is a PVD process in which surface particles are physically knocked off the source material, then condensing on the substrate. The depositing source, called the 'target,' is bombarded by energetic gaseous ions in 'plasma.' Kinetic energy from the incoming ions is transferred to the particles on the surface of the target, breaking the bonds between them and the bulk of the target. These surface particles are changed from solid to gas phase through the mechanical forces of the bombarding ions. Fig. 12 is a schematic of a basic sputtering system.

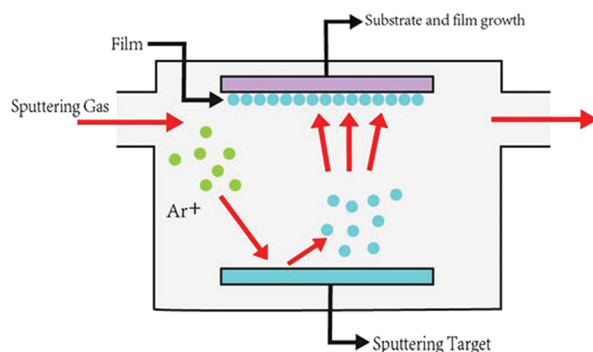


Fig. 12 Basic set-up of a sputtering system (<https://samaterials.wordpress.com/2015/10/28/what-is-sputtering/>).

The first crucial factor is the sputtering gas, which normally consists of ultrapure argon for non-reactive deposition or a mixture of argon with other reactive gas (O_2 , N_2 , CH_4 , H_2S , etc.) for reactive deposition. The sputtering gas mixture is ionized and turned to plasma through electrical discharge, which happens with the target as the cathode and the substrate as the anode. In this stage, the kinetic energy of ions in the plasma is dependent on the power of the electricity applied to the system. Subsequently, this also controls the kinetic energy of the sputtered particles. The operating pressure of the sputtering gas mixture is also important as it controls the flux of gaseous ions and thus the deposition rate. After being sputtered out of the target surface, ejected particles are deposited on the substrate, forming a thin film of the sputtered target, or of the product in the case of reactive sputtering. The properties of the thin film are greatly dependent on the structure and temperature of the substrate. Post-annealing can also be done after deposition to improve or change the quality of the deposited thin film. In summary, there are 4 main parameters that define a basic sputtering setup: (1) power supplied, (2) operating pressure, (3) substrate type, and (4) substrate temperature. For the same sputtering system, changes made to these parameters are the key to change and improve the thin film quality.

Currently, depending on the type of power supplied to the system during sputtering, there are several types of system, such as direct current sputtering, radio-frequency sputtering, magnetron sputtering, high-power impulse magnetron sputtering (HiPIMS), and ion-beam sputtering. Depending on the type of sputtering gas, systems can also be classified as either reactive or non-reactive sputtering. The methods to use these systems in depositing a VO_2 thin film are discussed in subsequent sections.

6.1. Reactive DC-magnetron sputtering (DCMS)

Reactive DC-magnetron sputtering is characterized by its three main features:

- (1) The sputtering gas is a combination of argon and reactive gas;
- (2) DC power is used as the electrical source for ionization during sputtering;
- (3) Magnetron sputtering is an add-on to the traditional system. It uses a magnetic field to trap and restrain electrons in

plasma longer, thereby creating more gaseous ions in plasma, subsequently enhancing the ionization rate and increasing the deposition rate of the system.

By using a DC power source, this technique is the lowest cost and simplest technique for metal deposition. However, this is also a limitation because only conductive materials can be used as the target.

In the case of VO_2 deposition, vanadium is a suitable target as a transition metal, and a mixture of argon and oxygen can be used as the reactive sputtering gas. Vanadium is known for its various oxidation states (II to V) so it is important to achieve the correct oxidation state for VO_2 . According to Kang,¹¹⁷ the composition of a VO_x system can be influenced by the temperature during deposition and the mole fraction of V and O. Despite knowing the required mole fraction from the literature, it is hard to achieve perfect VO_2 deposition in practice due to the lack of control between the ratio of sputtered vanadium and oxygen in the gas mixture. Thus, factors such as the O_2/Ar ratio, overall operation pressure, substrate temperature, and structure are tuned so that the V/O mole fraction can be controlled. Fig. 13 is the phase diagram of VO_x as a function of substrate temperature and oxygen partial pressure reported by Griffiths and Eastwood in 1974.¹¹⁸ This gives a general idea of how each stated parameter affects the phases in a sputtered VO_x film. The detailed effects of each parameter are discussed in the following sections.

Without a post-annealing process. Without any post-annealing process, the effects of factors such as the reactive gas ratio and substrate temperature can be observed more clearly. Yuce *et al.* fabricated a VO_2 thin film on a c-cut sapphire ($Al_2O_3(0001)$) substrate by optimizing the reactive oxygen flow ratio (Fig. 14b) while keeping constant the 550 °C substrate temperature, 50 W power and 0.85 Pa operational pressure.¹¹⁹ Raman spectra of the

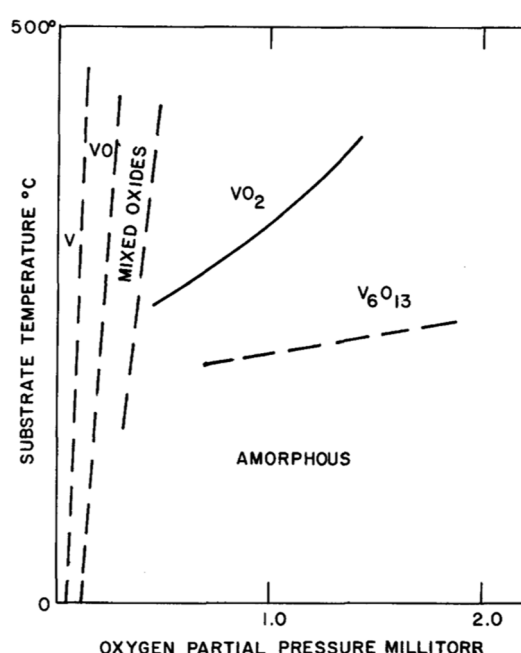


Fig. 13 Phase diagram of VO_x .

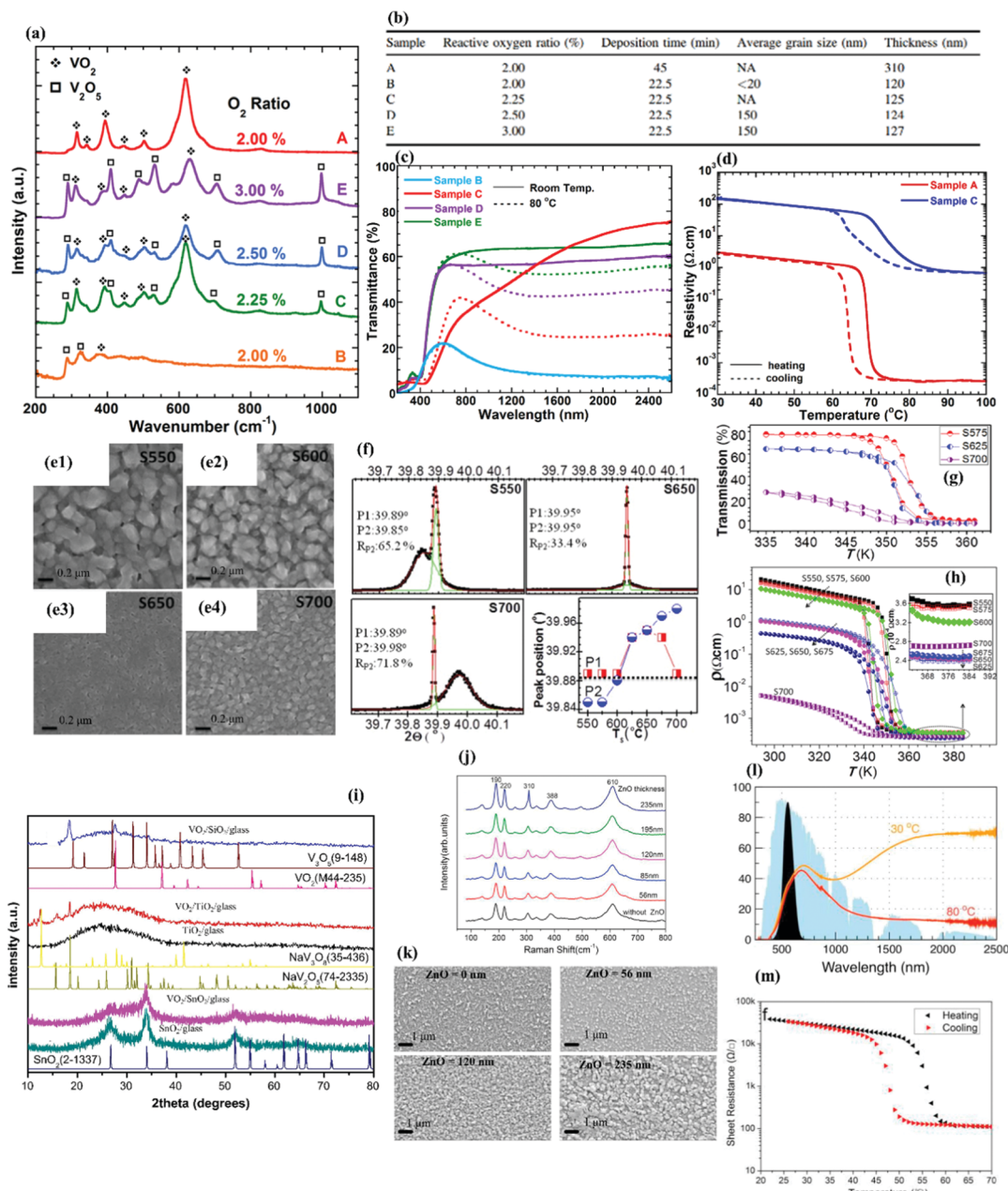


Fig. 14 Characterization of VO₂ deposited by reactive DCMS without annealing. (a and b) Raman spectra of thin films produced at varying O₂/Ar flow ratios. (c) Optical and (d) electrical properties of samples in (a). (e) SEM images of VO₂ deposited with different substrate temperatures. (f) XRD spectra of samples in (e). (g) Optical and (h) electrical properties of samples in (e). (i) XRD spectra of VO₂ on different substrates. (j) Raman spectra of VO₂ on different ZnO thicknesses. (k) SEM images of samples in (j). (l) Optical and (m) electrical properties of VO₂ on a 235 nm ZnO buffer layer.

thin films in Fig. 14a show a direct correlation between the increased presences of V₂O₅ in the deposited film and the increasing oxygen flow ratio. This is consistent with how a higher ratio of reactive oxygen flow (2.50–3.00%) leads to a higher oxygen mole fraction, which then results in a higher oxidation state of vanadium after reaction. Vanadium(v) was formed instead of vanadium(iv). The optical properties and electrical properties (Fig. 14c and d) of the deposited VO₂ also confirmed the abundant of VO₂ at 2.25% O₂ as the MIT was clear at this level but was not significant at a higher oxygen level. It can be

concluded that the flow ratio of O₂ directly affects the O₂ mole fraction and thus, the phase formation of VO_x.

Zhao *et al.* conducted an experiment in which seven samples of VO₂ films of 120 nm thickness were produced on a c-sapphire substrate at different substrate temperatures from 550 °C to 700 °C, while the other parameters were kept constant (0.4 Pa, 11% O₂/Ar flow ratio).¹²⁰ From the SEM images (Fig. 14e), the samples could be divided into 3 three representative groups: G1, G2 and G3. G1 (S550, S575 and S600) had a coarse, rough surface with a relatively larger grain size. It was reported that

G1 contained a porous structure as seen from the cross-section SEM images. G2 (S625 and S650) had a smooth surface and compact morphology with fine grains. On the other hand, G3 (675 and S700) had a rougher surface than G2 but less so than G1. According to the report, there was no porous structure detected in G3. These groupings in the microstructure also translated to differences seen in their XRD spectra. From Fig. 14f, the author concluded that the double peak in the XRD spectra could be attributed to the transition of vanadium oxide from $V^{5+} \rightarrow V^{4+} \rightarrow V^{3+}$ from low to high temperature. The presence of intermediate phases during the transition from V_2O_5 to VO_2 and from VO_2 to V_2O_3 was the main reason why there were double peaks in the XRD spectra. This result showed the influence of substrate temperature on the stoichiometry of the deposited vanadium oxide film.

A crucial aspect of any sputtering deposition set-up is the choice of substrate. c-cut sapphire was used by both Zhao *et al.* and Yuce *et al.* due to its ability to operate at high temperature, which was higher than 550 °C in both reports. In practice, soda-lime glass is a better substrate for testing because of its potential real-life application. However, soda-lime glass at high temperature exposes the thin film to the potential for the diffusion of sodium (Na) into the thin film, thus diminishing the transformation ability of VO_2 .

Zhu *et al.*¹²¹ deposited VO_2 on soda-lime glass substrate at the low temperature of 300 °C with 3 different buffer layers of TiO_2 , SnO_2 and SiO_2 . The other parameters did not deviate so much from other reported reactive DCMS set-ups: 80 W power, 0.55 Pa operation pressure, 3.25% O₂/Ar flow ratio. The XRD patterns in Fig. 14m show that TiO_2 is not a suitable buffer layer because it was not able to hinder the diffusion of Na into VO_2 , thus causing the detection of NaV_3O_8 and NaV_2O_5 . The SiO_2 -buffered sample showed the presence of (M) phase VO_2 with its characteristic peak. However, peaks from the V_3O_5 phase were also present. This means that the SiO_2 buffer layer did not manage to help create a pure VO_2 thin film. Only the SnO_2 buffered sample was relatively pure.

Zhu *et al.*¹²² proceeded further in this area by testing the deposition of VO_2 on different thicknesses of ZnO-coated soda-lime glass in order to investigate the effect of the buffer layer thickness on deposited VO_2 . A low temperature of 320 °C was used, with the other typical parameters being constant: 120 W power, 0.5 Pa operational pressure, and 4.5% O₂/Ar flow ratio. It was found that a thicker buffer layer promoted the crystallinity of VO_2 at a low substrate temperature. This could be observed by comparing the SEM image of VO_2 with and without different ZnO buffer thicknesses in Fig. 14l and m.

The studies discussed in this section are representative of work in this field and included here to demonstrate the effect of having a buffer layer on VO_2 thin films. Other materials have also been used as buffer layers in other studies and are discussed in a later section.

With a post-annealing process. Post-annealing in reactive DCMS is typically an extra step to guarantee the quality of a deposited thin film. This is done to either crystallize an amorphous film, to continue the reaction in reactive gas without further

sputtering or to purge excessive reactive gas from a deposited film. Yu *et al.* deposited VO_2 film on a polished silicon substrate at room temperature using varying O₂/Ar flow ratios, 0.06 Pa operation pressure and 90 W power.¹²³ A low temperature of the substrate undoubtedly resulted in amorphous VO_2 , which required recrystallization at 400 °C for 1 h in a nitrogen atmosphere. Nitrogen was used as an inert gas so it would not affect the established stoichiometry of the amorphous VO_2 film. The atmospheric or ambient pressure also contributed to keeping the stoichiometry.

Not only used as a remedy to low-temperature depositions, post-annealing is also used to further improve the quality of VO_2 deposited at high temperature. Dou *et al.* reported comprehensive findings on this by conducting a 2-step annealing process on deposited VO_2 (m/a/r-plane sapphire, 2% O₂/Ar flow ratio, 1 Pa, 550 °C).¹²⁴ After deposition, VO_2 film was crystallized at 500 °C for 400 s in 220 Pa atmosphere, followed by air oxidizing in atmospheric pressure at 450 °C for 200 s, 400 s, 600 s and 1000 s. The XRD patterns (Fig. 15a) showed a significant decrease in VO_2 presence with the increase in air oxidizing time. As expected, the V_2O_5 presence also increased due to the further oxidation of vanadium to the V^{5+} state.

In contrast, Huang *et al.*¹²⁵ conducted a post-annealing process in an O₂-lacking environment to transform the mixed phase vanadium oxide obtained from deposition to purer stoichiometry VO_2 . In this report, vanadium oxide film was deposited in a 12.5% O₂/Ar flow ratio, 0.11 Pa operation pressure, 200 W power and 300 °C substrate temperature. XRD patterns of the deposited film revealed the presence of a mixed VO_2 and V_2O_5 phase. After annealing in an Ar atmosphere, the V_2O_5 was eliminated, as seen in the XRD patterns in Fig. 15b.

The atmosphere for the post-annealing process was the deciding factor for achieving a VO_2 thin film. An inert atmosphere could be used for the crystallization of an amorphous film and for purging the excessive reactive gas, while an oxygen-rich atmosphere can support the further oxidation of the film to reach the desirable stoichiometry.

VO_2 deposition on m-, a- and r-plane sapphire was also reported by Dou *et al.* Before annealing, different substrates yielded different thin film microstructures (Fig. 15c). After 1000 s of air oxidation, all three samples turned into a similar microstructure. However, MIT investigation of these samples (Fig. 15d and e) showed they slowly lost their transition ability as they were subjected to longer post-annealing time. The similar microstructure resulting from the longer annealing time was believed to be V_2O_5 , which agrees with XRD spectra in Fig. 15a.

While the effect of having different substrates may not last after annealing, the effect of different O₂/Ar flow ratios is reported to be conserved, as reported by Xu *et al.* In their report, VO_2 thin film was deposited on a Si(100) substrate at room temperature, 200 W power, 0.63 Pa and O₂/Ar ratios of 25%, 32.5%, 42.5% and 50%. The deposited film was annealed in vacuum for 2 h at 450 °C.¹²⁶ Based on the XPS spectra (Fig. 15f), it could be observed that the vanadium oxide undergoes oxidation from $V^{3+} \rightarrow V^{4+} \rightarrow V^{5+}$ with the increasing

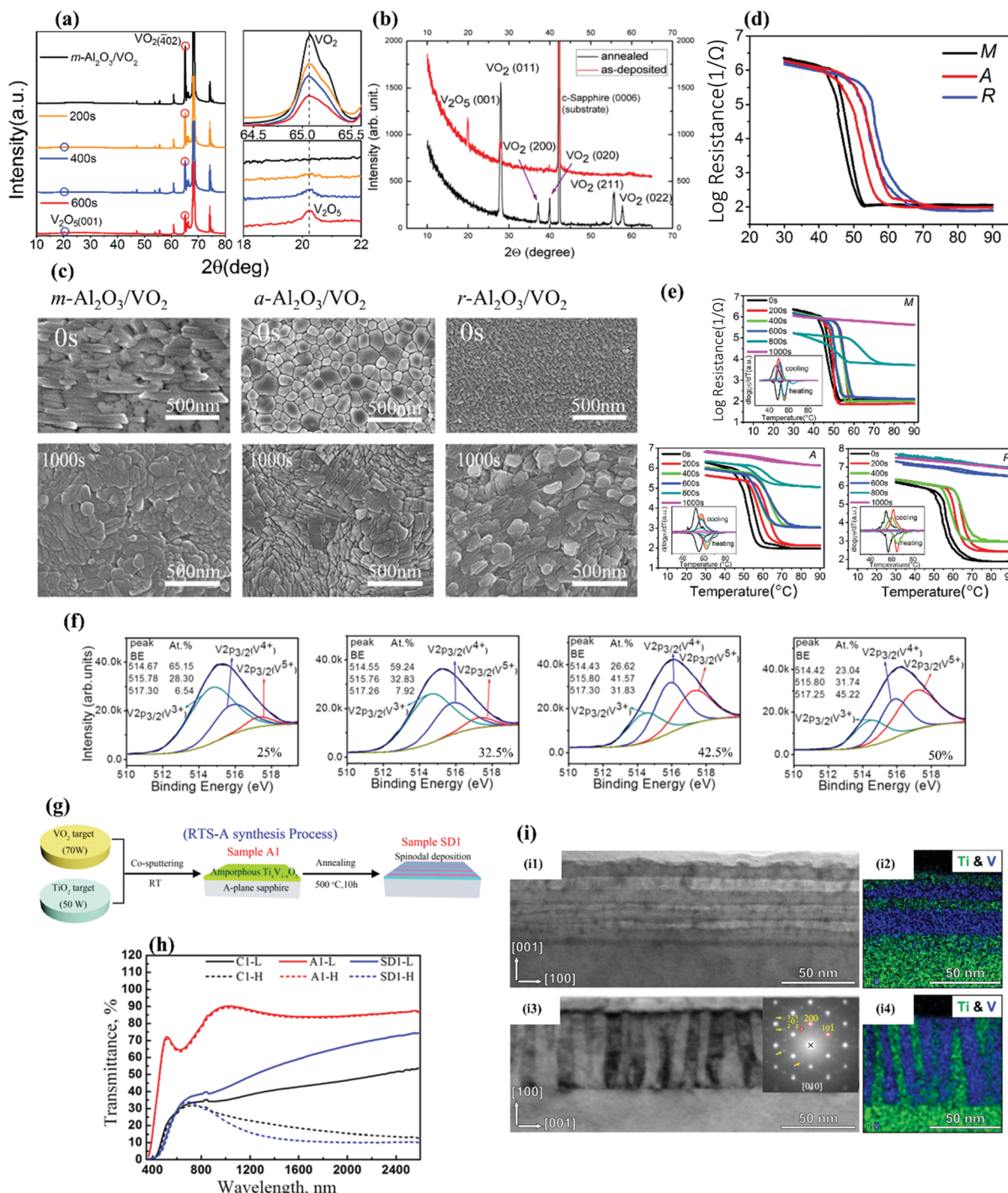


Fig. 15 Characterization of VO_2 thin film deposited by reactive DCMS with annealing. (a) XRD spectra of oxidized VO_2 on m-plane sapphire. (b) XRD patterns of vanadium oxide film before and after annealing. (c) SEM images of VO_2 samples on different substrates before and after 1000 s of annealing. Electrical properties of VO_2 samples in (c) before (d) and after (e) annealing. (f) XPS spectra of VO_2 thin film with different O_2/Ar ratios after annealing: 25%, 32.5%, 42.5%, and 50% respectively. (g) Spinodal decomposition process to achieve a $\text{TiO}_2\text{-VO}_2$ nanocomposite matrix. (h) Optical performance of A1 (sample fabricated by process in (g)), C1 (no annealed sample), V1 (pure VO_2 sample) by Sun et al. (i) Chen et al.'s work. (i1) and (i3) TEM images of the V-Ti separation after annealing, inset shows the SAED pattern. (i2 and i4) Combined STEM and energy-dispersive X-ray spectroscopy mapping of V-blue and Ti-green.

amount of O_2 . This is consistent with what was reported by Yuce *et al.* as mentioned in the previous section. It can be concluded that if the annealing time does not transform VO_2 to V_2O_5 , it has no influence on the effect of the different reactive gas flow ratios.

Post-annealing can be a powerful tool to remedy and correct the stoichiometry of the VO_x film or to complete the fabrication process. However, excessive annealing causes the formation of V_2O_5 from VO_2 and hinders the film MIT ability. Careful

planning for the annealing process is therefore needed to achieve a balance.

Aside from the traditional processes mentioned above, post-annealing can also be utilized to fabricate composite films of VO₂ through a spinodal decomposition mechanism. Sun *et al.*^{127,128} and Chen *et al.*¹²⁹ managed to fabricate a self-assembled multi-layer structure TiO₂-VO₂ thin film (Fig. 15g-i) by sputtering amorphous V_xTi_{1-x}O₂ at room temperature, followed by annealing this amorphous film to achieve a composite structure. The final matrix, as seen in Fig. 15i, had alternating V-rich and Ti-rich phases. As reported by Sun *et al.*¹²⁷ in Fig. 15h, the optical properties the VO₂ thin film were boosted significantly by doping with TiO₂ through this spinodal decomposition process.

6.2. Reactive RF-magnetron sputtering (RFMS)

The traditional sputtering system using DC power source is only capable of using conductive materials as the target. The need to sputter a wider range of materials thus led to the development of RF sputtering in which an alternate current (AC) is used as power source instead. This alternate current with a standard frequency of 13.56 MHz is used to create an alternate bias between the substrate and the target. By constantly changing the target as the cathode and anode, it prevents insulating the target to accumulate a positive charge over the course of sputtering. Thus, RF sputtering can be used for conducting, insulating and semiconducting materials. This means that metallic VO_x materials can be used as a sputtering target. This is further discussed in the non-reactive sputtering section.

Reactive RF-magnetron sputtering is very similar to its DC counterpart and so the traditional parameters, such as O₂/Ar flow ratio, substrate heating and substrate microstructure, still play crucial roles in deciding the quality of deposited films. However, using an AC power source allows generally a higher sputtering power to be used, ranging from 100 W¹³⁰ to as high as 450 W.¹³¹ This increased sputtering power also eliminates the annealing step in most reported papers, except when room temperature deposition is attempted.¹³²

Despite the similarity to its DC counterpart, the effects of conventional parameters are still investigated for VO₂ thin film deposited with reactive RF-magnetron. Jiang *et al.* reported investigations on a series of VO₂ samples on quartz glass at 450 °C with 200 W RF power under 1.0 Pa of varying O₂ flow.^{133,134} Instead of the traditional stoichiometry change with varying the O₂/Ar flow ratio, the report gave a fresh viewpoint on the effect of the O₂/Ar flow ratio on single-phase VO₂ thin film. While the XRD patterns (Fig. 16a) showed no signs of other vanadium oxide phases in the deposited thin film, AFM images (Fig. 16d) showed an increasing crystal size as the O₂/Ar flow ratio was increased from 2% to 5%. Variations in the optical properties and transition temperature (Fig. 16b and c) were also reported with an exceptional transition temperature of 46 °C for the 2% sample.

Some effects of different substrates and substrate temperatures were also reported. Panagopoulou *et al.* deposited VO₂ at 400 °C and 300 °C on various substrate materials: glass/ZnON, glass/SnO₂, commercial glass and a silicon substrate.¹³⁵ XRD analysis

(Fig. 16e and f) produced non-surprising results indicating a better-formed VO₂ using the higher substrate temperature of 400 °C. Broader peaks from the 300 °C samples provided evidence of secondary phases, whether different VO₂ phases or different VO_x stoichiometry, formed during deposition.

Aside from the traditional parameters, different methods to modify the sputtering process are also possible under RFMS. One of these is to create a secondary bias acting on the substrate concurrently with the RF acting on the target. Azhan *et al.* conducted a series of experiments using reactive RF-magnetron sputtering and RF substrate bias to deposit VO₂ on a single-crystal sapphire substrate.^{136,137} This set-up is shown in Fig. 16g. By using RF substrate bias during deposition, the reported transition temperature of the VO₂ film was 36 °C for 40 W biasing power. This is an extremely good value compared to the conventional transition temperature of 68 °C. However, films deposited with a higher biasing power showed significant decreases in MIT ability. A balance between the transition temperature and MIT properties is thus needed so that VO₂ films deposited by this method can be considered for further application.

6.3. Reactive pulsed direct current magnetron sputtering (pDCMS)

Pulsed direct current magnetron sputtering is the result of combining the DC power source from conventional DCMS and the concept of alternating bias to prevent target charging from RFMS. Instead of using an AC power source with frequency in the range of MHz, pDCMS still uses a DC power source with a pulsing capability in the range of kHz. This prevents charge accumulation on the insulator target surface, allowing a wider range of materials to be used with a DC power source. Additional systems, such as substrate bias, can also be used in this case while being traditionally redundant in conventional DCMS.¹³⁸

6.4. Reactive high-power impulse magnetron sputtering (HiPIMS)

High-power impulse magnetron sputtering or HiPIMS is a recently developed technology that combines magnetron sputtering and pulsed power. Similar to how DC and RF sputtering are characterized by their method to create plasma from the sputtering gas, HiPIMS is characterized by the use of high voltage and a short duration energy burst (pulse) to generate plasma. Because of this plasma generation mechanism, high-density plasma can be formed on the surface of target materials, causing a higher degree of ionization of the sputtered particles as well as a higher rate of molecular gas dissociation compared to other sputtering methods. In other words, an HiPIMS deposited thin film often has a higher density than films from other methods.

Using HiPIMS for VO₂ deposition is still a relatively new research area. Due to the theoretical higher film density, it is expected that high-quality VO₂ could be deposited with much lower temperature (<400 °C) compared to its DC and RF counterpart without using any post-annealing process. This allows for a wider range of substrate selection; even a polymeric substrate has been attempted.¹³⁹ Aside from the conventional parameters like in other previously mentioned reactive sputtering methods, HiPIMS systems are also identified by the

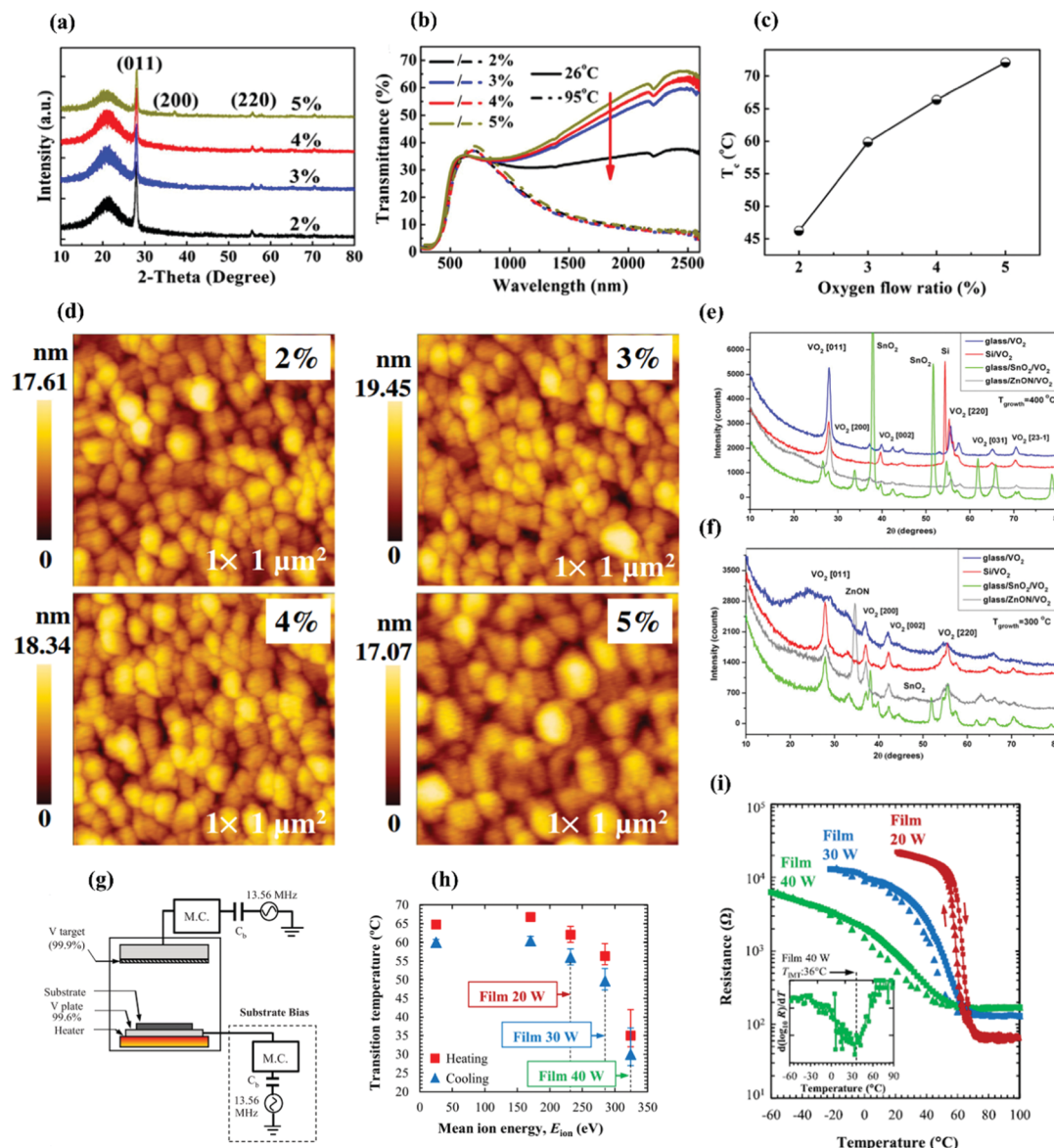


Fig. 16 Characterization of VO_2 deposited by RFMS: (a) XRD patterns, (b) transmission spectra, (c) transition temperature for each sample, (d) AFM images of each sample, (e and f) XRD of VO_2 deposited on different substrates at different temperatures. (g) RFMS with RF substrate bias set-up. (h) Transition temperature and (i) electrical properties changes of VO_2 thin film against the substrate bias applied.

frequency and duty cycle of their pulses. Sadly, there has been no report yet on the effect of these parameters on similarly prepared VO_2 samples. HiPIMS systems are compatible with additional substrate bias. Results both with^{131,138–140} and without¹⁴¹ substrate bias have been reported.

HiPIMS vs. RFMS. Loquai *et al.* conducted a comparison between VO_2 deposited on B270 glass using HiPIMS and RFMS.¹³⁹ The processing parameters utilized, as seen in Fig. 17a, were comparable between both deposition processes, except for a different O_2/Ar flow ratio. From the transmission spectra (Fig. 17b and c), the optical properties of VO_2 film by both depositions processed were also similar despite the difference in O_2 flow. This means that HiPIMS could produce similar grade VO_2 with half the amount of O_2 as compared to RFMS.

HiPIMS vs. pDCMS. Aijaz *et al.* conducted an extensive study on the effect of substrate temperature, O_2/Ar flow ratio and substrate bias on the quality of VO_2 thin films deposited by both HiPIMS and pDCMS.¹³⁸ An average power of 600 W was used for both HiPIMS (500 Hz, pulse on-time of 100 μs) and pDCMS (100 kHz, pulse off-time 1.6 μs). By using a measured discharge voltage against O_2 fraction plot (Fig. 17c), the point of transition between the metallic film and insulating film could be singled out. Thus, the stoichiometry of the VO_2 film could be identified. The thermochromic performance of VO_2 by HiPIMS at different O_2 fractions, temperature and substrate bias is shown in Fig. 17d. As concluded in previous sections, increasing the O_2 fraction leads to a transition from $\text{V}^{3+} \rightarrow \text{V}^{4+} \rightarrow \text{V}^{5+}$. This was reaffirmed in this report. Comparison with VO_2 by pDCMS

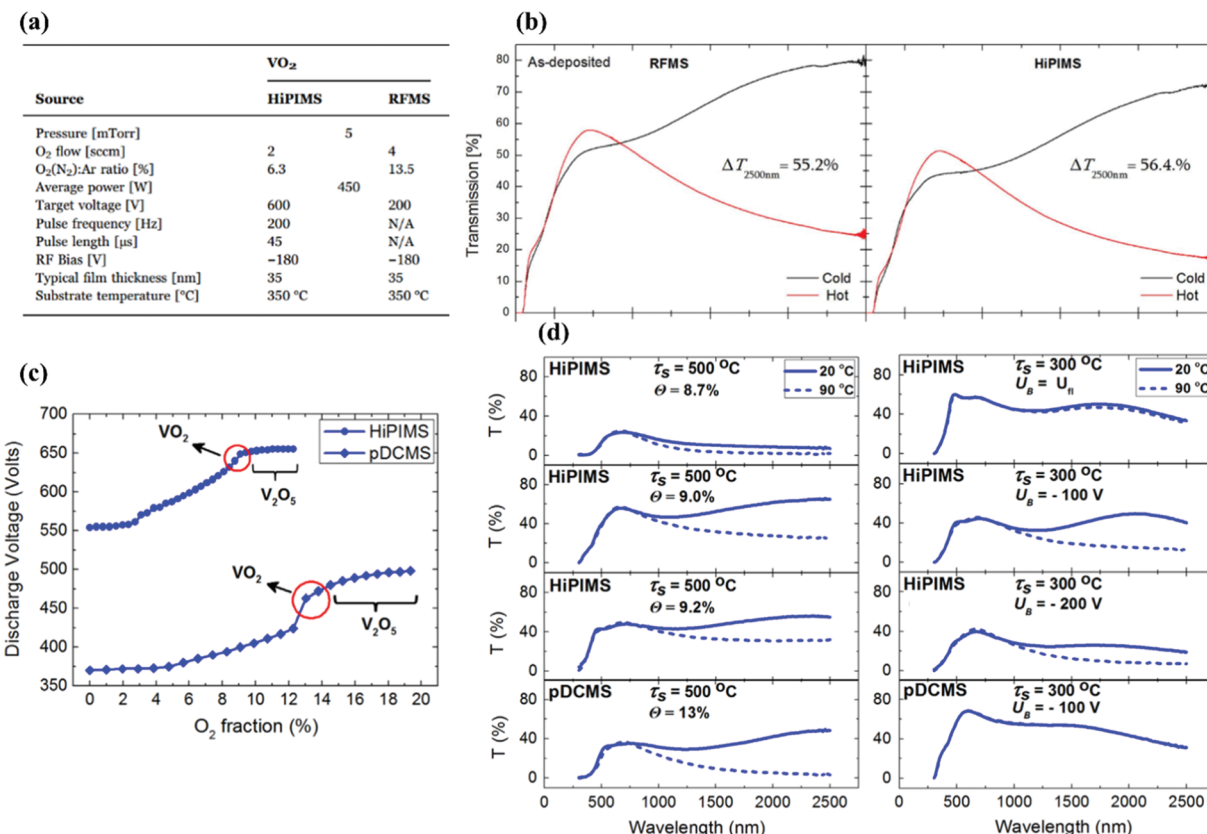


Fig. 17 (a) Deposition parameters and (b) optical properties of VO₂ thin film by RFMS and HiPIMS. (c) Measured discharge voltage during deposition vs. O₂ fraction. (d) Transmission spectra of VO₂ thin film with no bias and varying bias and a constant O₂ fraction of 8.7%.

showed that HiPIMS is able to produce functional thermochromic VO₂ at a much lower substrate temperature.

6.5. Inductively coupled plasma-assisted sputtering (ICPS)

ICPS is an unconventional modification to conventional sputtering methods. In addition to the magnetron plasma produced by a magnetic field near the target surface, conductive coils are installed in the space between the target and the substrate (Fig. 18a). This configuration can further enhance the plasma density during sputtering, reaching a density comparable to HiPIMS but without the use of extremely high energy pulses.

Reports on VO₂ deposition using ICPS are limited to a couple of research group due to the niche set-up.^{142–146} Mian and Okimura compared conventional RFMS and ICPS using low-temperature (250 °C) deposition and traditional temperature (400 °C).¹⁴² XRD spectra comparison (Fig. 18d and e) showed an exceptional quality of the VO₂ thin film deposited at 250 °C by ICPS. The XRD peaks from the 250 °C samples from both the ITO and Si substrate were comparable, even sharper than the 400 °C peaks by conventional RFMS.

6.6. Inverted cylindrical magnetron sputtering (ICMS)

ICMS is another modification of the conventional RFMS set-up. Instead of additional magnetic coils, like in ICPS, a perpendicular cathode and anode set-up is used (Fig. 18b). This set-up is useful for deposition on a substrate with a complex geometry. Aside from

this niche usage, other parameters for ICPS do not deviate too much from conventional RFMS. Research on VO₂ deposition by ICPS is rare but the reported results to date are comparable to those achieved with a conventional system.^{147,148}

6.7. Ion-beam-assisted sputtering (IBS)

Ion-beam-assisted sputtering is different from all the previously discussed sputtering methods. Instead of generating bombarding ions inside a plasma of sputtering gas mixture, ions are directly propagated towards target materials at an angle so that ejected particles are deposited on the substrate surface (Fig. 18c). Because ions are injected into the chamber using ion guns, the operating pressure in an IBS system is much lower than that in conventional plasma sputtering. IBS has the advantage of controlling the stoichiometry of the deposited film by tuning the power of the ion guns. This is especially useful for hard-to-control stoichiometry compounds, such as VO_x. However, IBS is still mainly used for the non-reactive sputtering of vanadium metal thin films instead.^{149,150} Reactive IBS requires a dual ion-gun configuration to control O₂ and Ar separately.¹⁵¹

6.8. Non-reactive sputtering methods

A non-reactive VO₂ sputtering system either uses a VO_x ceramic target as the source material or consists of 2 steps: deposition of a vanadium metal thin film on a substrate, and oxidation of the said film into VO₂.

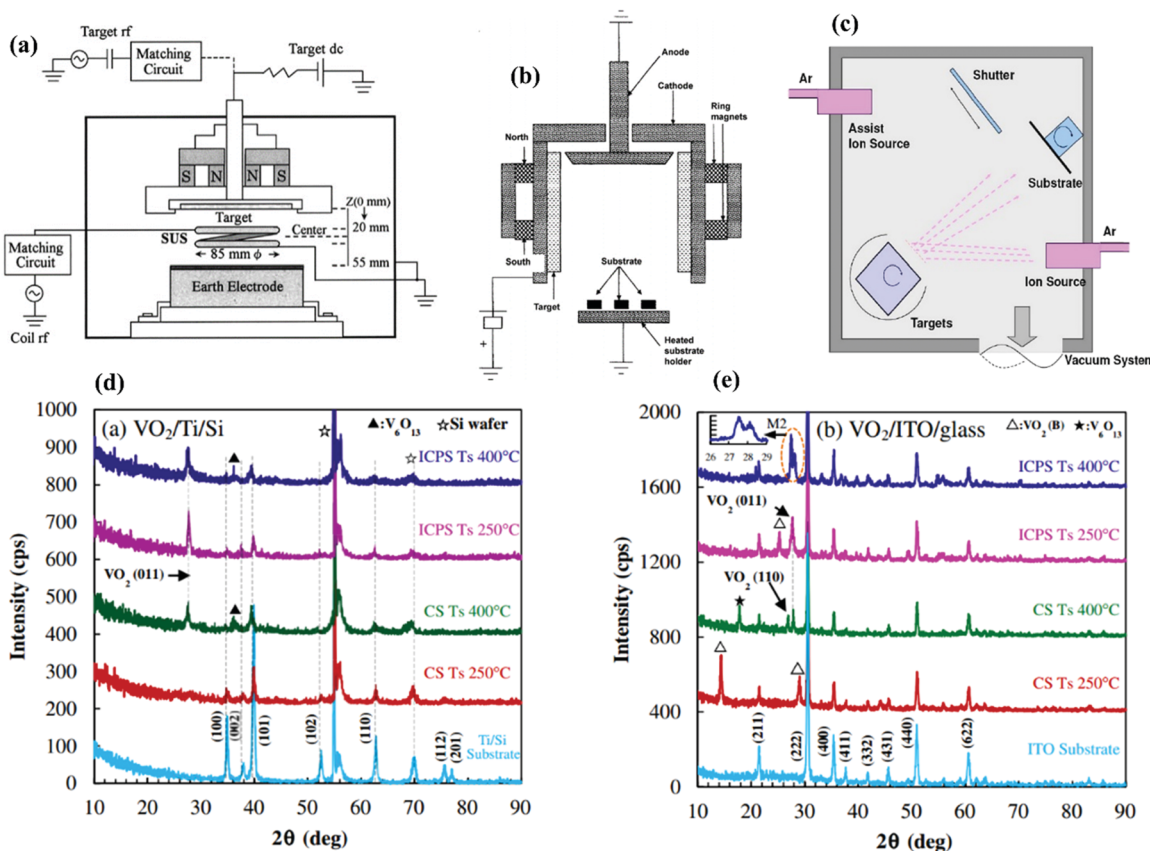


Fig. 18 (a) Schematic of an ICPS system. (b) Schematic of an ICMS system. (c) Schematic of an ion-beam-assisted sputtering system. XRD spectra of VO₂ on Ti/Si substrate (d), and on an ITO/glass substrate (e).

Ceramic target system. As mentioned in the previous section, the molar ratio of vanadium and oxygen during sputtering is one of the most crucial factors to achieve stoichiometric VO₂. A method to bypass this issue is to use a VO₂ ceramic target as the source material during sputtering. Theoretically, the vanadium to oxygen ratio in the produced film should be the same as in the source. Yu *et al.* reported a typical process to produce stoichiometric VO₂ using this method.¹⁵² Non-reactive RFMS was used to sputter VO₂ ceramic onto Eagle XG glass with a pure Ar atmosphere. Post-annealing was done under vacuum to enhance the thin film crystallinity. As expected, RFMS was used due to it being the most common system for ceramic sputtering. This is because most ceramics are insulators and are not suitable to be sputtered using a DC power. However, VO₂ is unique because it exhibits metallic properties at room temperature. Thus, DCMS was also attempted and shown to be successful by Sun *et al.*¹⁵³ VO₂ is not the only ceramic target that can be used as a thin film source, and a V₂O₅ target has also been tested.¹⁵⁴ Due to having a different stoichiometry, an additional annealing process in an O₂-rich environment is required to reach the final VO₂ thin film.

Vanadium target system with pure argon sputtering. A VO₂ thin film can also be achieved through the oxidation of a sputtered vanadium film. DCMS is the most common method to produce a vanadium film as it is the cheapest and most accessible

sputtering system.^{155–160} There are also reports, however, on IBS being used instead.^{149,150} The deposition of a vanadium film is applicable for a wide range of substrates because it is common practice to conduct deposition at room temperature on a substrate. The crystallinity and morphology of the as-deposited vanadium film are not the emphasis of these studies. Most of them instead have been focused on the effect of the annealing and oxidation parameters on the final VO₂ film. Details are not discussed here as they are not the focus of this paper. However, it is important to note that this is one of the main synthesis routes of a VO₂ film through a sputtering system.

7. Strategies to improve the performance of VO₂ thin films using PVD

As discussed in the beginning of this review, VO₂ is not a perfect material and the multiple intrinsic limitations of VO₂ need to be addressed before it can be applied commercially. Over the years, concurrently with attempts to fabricate high-quality pure VO₂, various strategies have been developed to modify the matrix to improve its feasibilities. Each of the following strategies is proposed to solve at least one of the main problems of pure VO₂, namely the high transition temperature τ_C , low T_{lum} and ΔT_{sol} , and substrate effects.

7.1. Elemental doping

The deposition of VO_2 was performed to investigate its MIT properties with different fabrication parameters and conditions. In order to manipulate the transition temperature of VO_2 , the doping of various elements into the VO_2 matrix has become a common strategy. Table 1¹⁶¹ shows a non-exhaustive list of the dopants that have been investigated over the years and their effects on the intrinsic properties of VO_2 . Tungsten is the most common dopant due to its ability to greatly reduce the transition temperature of VO_2 at the expense of reduced optical properties. Therefore, reports of doped VO_2 have mainly focused on W,^{161–163} followed by Al,¹⁶⁴ Mg^{161,165–167} and surprisingly Si.^{168,169} DCMS and RFMS are most common methods used to fabricate doped VO_2 . For these processes, there are multiple methods where the dopant amount can be controlled:

(1) A limited amount of dopant can be attached to vanadium target during sputtering. An equal sputtering power is applied on the target and dopant pellets. The dopant amount in the film is controlled through the number of pellets used.^{162,164,165,168,169} This is the most common set-up as a single-target configuration with one power source is applicable.

(2) The dopant and vanadium can also be co-sputtered as two targets, using different power sources.^{166,167} This is less common due to the limited accessibility of the co-sputtering configuration.

(3) An alloy of a dopant with vanadium can also be used as a sputtering target.¹⁶³ This is the least common method due to the limited choice of dopant and the dopant ratio that can be tested.

(4) An amorphous solid solution of a dopant and vanadium can be co-deposited on the substrate, followed by annealing to spinodally decompose the matrix into a nano-composite structure. Similar systems and crystal structures are needed for this to be possible.¹²⁷

Aside from the common rare earth elements and transition metals listed in Table 1, noble metals, such as Au^{170,171} and Ag,^{172–174} have been studied as potential doping elements in recent years. The surface plasmon resonance (SPR) properties exhibited by those elements at the near-IR-vis wavelength open up the possibilities of localized heating to decrease the τ_{C} of the VO_2 matrix.

7.2. Multilayer structures

Buffer layer. As mentioned in previous sections of the review, the usage of buffer layers has been an integral part of

Table 1 Effects of selected doping on the optical properties of VO_2

Dopant	Limit	Effect on τ_{C}	Effect on T_{lum}	Effect on ΔT_{sol}
Eu^{3+}	4 at%	↓ 6.5 °C/at%	↑	↑
Mg^{2+}	7 at%	↓ 3 °C/at%	↑	↑
W^{8+}	2.5 at%	↓ 23 °C/at%	↓	↓
F^-	2.1 at%	↓ 20 °C/at%	N.A.	N.A.
Mo^{6+}	2.5 at%	↓ 12 °C/at%	↑	↓
Nb^{5+}	4 at%	↓ 8 °C/at%	↓	↓
P^{3-}	1 at%	↓ 13 °C/at%	N.A.	N.A.
Fe^{3+}	1.4 at%	↓ 6 °C/at%	N.A.	N.A.
Sb^{3+}	7 at%	↓ 1 °C/at%	↑	N.A.
Zr^{4+}	11 at%	N.A.	↑	↑

the deposition process of VO_2 . Buffer layers serve as a shortcut to broaden the possibilities of the surfaces to grow a VO_2 thin film while keeping glass as the main backing material. The usage of any kind of buffer layers is largely to offset negative effects caused by the chosen substrates on the performance of VO_2 thin films. Typically, it acts as a diffusion barrier to prevent impurities from the substrates, such as sodium ions in soda lime glass, from diffusing into VO_2 during deposition, and it can also be used as the basis for the epitaxial growth of a VO_2 thin film as well as a seed layer that can facilitate the crystallization of VO_2 under unconventional deposition conditions, such as low deposition temperature.^{121,122,175–177} Several studies on different compounds, including but not limited to SiN_x ,¹⁷⁵ ZnO ,^{121,122,176} V_2O_3 ,^{177,178} TiO_2 ,^{121,176} and SnO_2 ,^{121,176,179} have been done focusing solely on these two benefits of having a buffer layer.

However, some compounds push the advantages of buffer layers further than just being a seed layer or a diffusion barrier. Montero *et al.*¹⁷⁹ used $\text{In}_2\text{O}_3:\text{Sn}$ (ITO) as a conductive layer on soda lime glass to enhance the effect of substrate bias during the RFMS deposition of a VO_2 thin film. In this study, a buffer layer was used to expand the fabrication condition of VO_2 , activating an otherwise insulating material as a suitable substrate. Other researchers attempted to directly improve the performance of VO_2 thin film with an appropriate buffer layer. For instance, Chang *et al.*¹⁸⁰ successfully showed that a Cr_2O_3 buffer layer could enhance the optical properties of VO_2 thin film, achieving respectable values of $\Delta T_{\text{sol}} = 12.2\%$ and $T_{\text{lum}} = 46.0\%$, which were enhanced by 4.4% and 9.6% compared with pure VO_2 .

Antireflection coating and multilayers structure. Because buffer layers are largely used as a strategy to achieve high-quality VO_2 thin films, their effect on the optical performance of VO_2 is mostly indirect and unrecognized in most studies utilizing them. This is due to the upper most layer of the matrix still being VO_2 . The interaction with incident light is mostly unmodified with or without a buffer. Hence, an antireflection (AR) coating has been adopted as a strategy to improve the optical properties (ΔT_{sol} and T_{lum}) as well as to reduce interaction between O_2 in the atmosphere with VO_2 thin film, which has been proven to be easily oxidized to V_2O_5 with prolonged uncontrolled exposure.¹⁸¹ Combining the AR coating and buffer layers into a VO_2 matrix opens up more avenues for development. The properties of the VO_2 matrix are more flexible as they are now dependent on changes to not only the VO_2 thickness and crystallinity but also to the type of buffers, type of AR coatings, and their thickness, respectively. A non-exhaustive summary of studies using AR coatings and multilayers structure is listed in Table 2. It is observed that there is a delicate balance between the enhancement of T_{lum} and ΔT_{sol} . An increment of one parameter usually comes with the sacrifice of the other one. It is crucial for studies to understand this relationship and to achieve a balance of these two parameters.

8. Recommendations and future work

Despite the extensive efforts by several research groups all over the globe in recent years, VO_2 thin films for smart window

Table 2 Optical performance enhancement of selected VO₂ system using AR coating

Buffer layer	AR coating	Effect on T_{lum}	Effect on ΔT_{sol}	Ref.
—	ZrO ₂	↑18.2%	—	182
—	Al _x O _y	—	—	183
TiO ₂	TiO ₂	↓2.9%	↑1.6%	184
		↑16.9%	↑1.5%	185
		↑3.2%	↑5.4%	
		↑0.6%	↑3.9%	186
		↑24.9%	↓1%	187
		Highest ↑6.65%	Highest ↑3.4%	188
SiN _x	SiN _x	↑17.4%	↓1.8%	189
WO ₃	WO ₃			

application are still largely theoretical and only feasible in a laboratory environment. PVD in general is an effective approach to deposit VO₂ due to its relative simplicity to control the stoichiometry, high crystallinity and high performance. However, the high temperature and high-vacuum conditions required for the deposition continue to be a hindrance to the mass production of VO₂-based materials for commercial usages.

While they can easily be fabricated nowadays, the optical and thermochromic performances of VO₂ thin films continue to be a significant roadblock.¹⁹⁰ At this moment, while it is possible to achieve a near room temperature τ_c for VO₂ thin films through doping, it often comes with it a sacrifice to either T_{lum} or ΔT_{sol} due to the resulting impurities and irregularities in the films caused by the introduction of foreign atoms into the matrix. Meanwhile, T_{lum} and ΔT_{sol} have been increased by a variety of methods with limited effects, such as a multi-layered architecture (*i.e.* buffer layers,^{121,122,135,143,166,168} or sandwich structure¹⁸¹) or by the nano-patterning of VO₂.^{191,192} However, it is of utmost important for all these three key parameters to be improved simultaneously. Further studies into VO₂ performance optimization should adhere to this line of thought. On the other hand, the addition of functional layers onto the VO₂-based smart window architecture has opened up the question of whether multi-functional smart windows can be achieved. Further research into this area by adding sub-functions, such as self-cleaning or self-healing ability, would keep VO₂-based smart windows competitive among the energy conservation research landscape and functional windows.^{193–197}

It is to be noted that most studies about VO₂ focus on material properties and ignore the product feasibility aspect of smart windows. Currently, most deposition of high-quality VO₂ thin films is limited to experimental substrates, such as fused silica, and the transition to regular soda-lime window glass is still a challenge due to the issue of sodium's diffusion and substrate mismatch. A method to circumvent this is to insert buffer layers, but this is complicated and detrimental to the crystal formation. Furthermore, the mass production of VO₂ coating is still in its infancy and more effort is required to reduce the deposition temperature and enhance the crystallinity and design of the multifunctional layers.

In conclusion, it is crucial to continue to increase the performance of VO₂ thin films as a thermochromic material as well as to bridge the gap between the laboratory standards and industry large-scale production. Continuing efforts to

reduce the deposition temperature, enhance the crystallinity and uniformity as well as performance improvement and upscaling are needed to promote the commercialization of VO₂ in thermochromic smart window applications.

Conflicts of interest

There are no conflicts to declare.

Acknowledgements

Dr Long and Prof. Gao designed the outline. T. D. V., Dr Long, and Dr Liu wrote sputtering section and strategies to improve (Sections 6 and 7). Dr Chen and Prof. Gao wrote evaporation sections (Sections 2–5). T. D. V. and Dr Long wrote the abstract, introduction, and conclusions. Dr Zeng read through the paper and advised accordingly. This research was supported by the Ministry of Science and Technology of China (2016YFB0303901), Singapore Minister of Education (MOE) Academic Research Fund Tier one RG200/17, and the National Research Foundation, Prime Minister's Office, Singapore, under its Campus for Research Excellence and Technological Enterprise (CREATE) program, the National Natural Science Foundation of China (51702209, 51702208, 51873102), and the Shanghai Municipal Science and Technology Commission (18JC1412800).

Notes and references

- 1 A. M. Omer, *Renewable Sustainable Energy Rev.*, 2008, **12**, 2265–2300.
- 2 S. Lemmet, *United Nations Environmental Programme, Sustainable Buildings and Climate Initiative*, Paris, 2009, pp. 1–62.
- 3 L. Pérez-Lombard, J. Ortiz and C. Pout, *Energy Build.*, 2008, **40**, 394–398.
- 4 C. K. Cheung, R. J. Fuller and M. B. Luther, *Energy Build.*, 2005, **37**, 37–48.
- 5 A. Synnefa, M. Santamouris and H. Akbari, *Energy Build.*, 2007, **39**, 1167–1174.
- 6 M. Kamalisarvestani, R. Saidur, S. Mekhilef and F. S. Javadi, *Renewable Sustainable Energy Rev.*, 2013, **26**, 353–364.
- 7 R. Baetens, B. P. Jelle and A. Gustavsen, *Sol. Energy Mater. Sol. Cells*, 2010, **94**, 87–105.
- 8 M. Tarantini, A. D. Loprieno and P. L. Porta, *Energy*, 2011, **36**, 2473–2482.
- 9 Y. Cui, Y. Ke, C. Liu, Z. Chen, N. Wang, L. Zhang, Y. Zhou, S. Wang, Y. Gao and Y. Long, *Joule*, 2018, **2**, 1707–1746.
- 10 T. L. Cocker, L. V. Titova, S. Fourmaux, G. Holloway, H. C. Bandulet, D. Brassard, J. C. Kieffer, M. A. El Khakani and F. A. Hegmann, *Phys. Rev. B: Condens. Matter Mater. Phys.*, 2012, **85**, 155120.
- 11 Y. Ke, C. Zhou, Y. Zhou, S. Wang, S. H. Chan and Y. Long, *Adv. Funct. Mater.*, 2018, **28**, 1800113.
- 12 Y. Ke, S. Wang, G. Liu, M. Li, T. J. White and Y. Long, *Small*, 2018, **14**, 1802025.

- 13 S. Y. Li, G. A. Niklasson and C. G. Granqvist, *Thin Solid Films*, 2012, **520**, 3823–3828.
- 14 Y. Gao, S. Wang, H. Luo, L. Dai, C. Cao, Y. Liu, Z. Chen and M. Kanehira, *Energy Environ. Sci.*, 2012, **5**, 6104–6110.
- 15 S. Wang, K. A. Owusu, L. Mai, Y. Ke, Y. Zhou, P. Hu, S. Magdassi and Y. Long, *Appl. Energy*, 2018, **211**, 200–217.
- 16 N. Wang, M. Duchamp, C. Xue, R. E. Dunin-Borkowski, G. Liu and Y. Long, *Adv. Mater. Interfaces*, 2016, **3**, 1600164.
- 17 J. Zhou, Y. Gao, X. Liu, Z. Chen, L. Dai, C. Cao, H. Luo, M. Kanahira, C. Sun and L. Yan, *Phys. Chem. Chem. Phys.*, 2013, **15**, 7505–7511.
- 18 I. Mjejri, N. Etteyeb and F. Sediri, *Ceram. Int.*, 2014, **40**, 1387–1397.
- 19 C. Liu, X. Cao, A. Kamyshny, J. Y. Law, S. Magdassi and Y. Long, *J. Colloid Interface Sci.*, 2014, **427**, 49–53.
- 20 C. Liu, N. Wang and Y. Long, *Appl. Surf. Sci.*, 2013, **283**, 222–226.
- 21 Q. Lu, C. Liu, N. Wang, S. Magdassi, D. Mandler and Y. Long, *J. Mater. Chem. C*, 2016, **4**, 8385–8391.
- 22 S. Swann, *Phys. Technol.*, 1988, **19**, 67.
- 23 S. M. Rossnagel, *J. Vac. Sci. Technol., A*, 2003, **21**, S74–S87.
- 24 Q. Wei, Y. Xu and Y. Wang, in *Surface Modification of Textiles*, ed. Q. Wei, Woodhead Publishing, 2009, pp. 58–90, DOI: 10.1533/9781845696689.58.
- 25 J. Nag and R. F. Haglund, Jr., *J. Phys.: Condens. Matter*, 2008, **20**, 264016.
- 26 M. Borek, F. Qian, V. Nagabushnam and R. K. Singh, *Appl. Phys. Lett.*, 1993, **63**, 3288–3290.
- 27 M. Borek, F. Qian, V. Nagabushnam and R. K. Singh, *Appl. Phys. Lett.*, 1993, **63**, 3288–3290.
- 28 M. Soltani, M. Chaker, E. Haddad, R. V. Kruzelecky and J. Margot, *Appl. Phys. Lett.*, 2004, **85**, 1958–1960.
- 29 J. Nag, R. F. Haglund, Jr. and E. A. Payzant, in *2011 Conference on Lasers and Electro-Optics*, IEEE, 2011.
- 30 H. Kim, N. Charipar, M. Osofsky, S. B. Qadri and A. Pique, *Appl. Phys. Lett.*, 2014, **104**, 081913.
- 31 T.-H. Yang, W. Wei, C. Jin and J. Narayan, in *Materials and Devices for Smart Systems III*, ed. J. Su, L. P. Wang, Y. Furuya, S. TrolierMcKinstry and J. Leng, 2009, vol. 1129, pp. 325–334.
- 32 J. Lappalainen, S. Heinilehto, H. Jantunen and V. Lantto, *J. Electroceram.*, 2009, **22**, 73–77.
- 33 B. N. Masina, S. Lafane, L. Wu, S. Abdelli-Messaci, T. Kerdja and A. Forbes, *Opt. Eng.*, 2015, **54**, 73–77.
- 34 Y. X. Guo, Y. F. Liu, C. W. Zou, Z. M. Qi, Y. Y. Wang, Y. Q. Xu, X. L. Wang, F. Zhang and R. Zhou, *Appl. Phys. A: Mater. Sci. Process.*, 2014, **115**, 1245–1250.
- 35 S. Lafane, T. Kerdja, S. Abdelli-Messaci, Y. Khereddine, M. Kechouane and O. Nemraoui, *Appl. Phys. A: Mater. Sci. Process.*, 2013, **112**, 159–164.
- 36 L. L. Fan, Y. F. Wu, C. Si, C. W. Zou, Z. M. Qi, L. B. Li, G. Q. Pan and Z. Y. Wu, *Thin Solid Films*, 2012, **520**, 6124–6129.
- 37 D. H. Kim and H. S. Kwok, *Appl. Phys. Lett.*, 1994, **65**, 3188–3190.
- 38 F. J. Morin, *Phys. Rev. Lett.*, 1959, **3**, 34–36.
- 39 B. D. Ngom, M. Chaker, A. Diallo, I. G. Madiba, S. Khamlich, N. Manyala, O. Nemraoui, R. Madjoe, A. C. Beye and M. Maaza, *Acta Mater.*, 2014, **65**, 32–41.
- 40 M. Soltani, M. Chaker, E. Haddad and R. V. Kruzelecky, *J. Vac. Sci. Technol., A*, 2006, **24**, 612–617.
- 41 M. Maaza, K. Bouziane, J. Maritz, D. S. McLachlan, R. Swanepool, J. M. Frigerio and M. Every, *Opt. Mater.*, 2000, **15**, 41–45.
- 42 H. Liu, O. Vasquez, V. R. Santiago, L. Diaz and F. E. Fernandez, *J. Electron. Mater.*, 2004, **33**, 1171–1175.
- 43 J. Y. Suh, R. Lopez, L. C. Feldman and R. F. Haglund, *J. Appl. Phys.*, 2004, **96**, 1209–1213.
- 44 G. Xu, P. Jin, M. Tazawa and K. Yoshimura, *Appl. Surf. Sci.*, 2005, **244**, 449–452.
- 45 H. Zhou, J. Li, Y. Xin, G. Sun, S. Bao and P. Jin, *Ceram. Int.*, 2016, **42**, 7655–7663.
- 46 H. Zhou, X. Cao, M. Jiang, S. Bao and P. Jin, *Laser Photonics Rev.*, 2014, **8**, 617–625.
- 47 V. Thery, A. Boulle, A. Crunteanu and J. C. Orlianges, *Appl. Phys. Lett.*, 2017, **111**, 251902.
- 48 J. M. Bian, M. H. Wang, H. J. Sun, H. Z. Liu, X. X. Li, Y. M. Luo and Y. Z. Zhang, *J. Mater. Sci.*, 2016, **51**, 6149–6155.
- 49 A. Kar, N. Shukla, E. Freeman, H. Paik, H. C. Liu, R. Engel-Herbert, S. S. N. Bhardwaja, D. G. Schlom and S. Datta, *Appl. Phys. Lett.*, 2013, **102**, 5.
- 50 Y. Yang, S. Long, G. Sun, Z. Shao, P. Jin and X. Cao, *Jpn. J. Appl. Phys.*, 2018, **57**, 100303.
- 51 A. Srivastava, H. Rotella, S. Saha, B. Pal, G. Kalon, S. Mathew, M. Motapothula, M. Dykas, P. Yang, E. Okunishi, D. D. Sarma and T. Venkatesan, *APL Mater.*, 2015, **3**, 026101.
- 52 J. Yang, Z. Xu, H. Ye, X. Xu, X. Wu and J. Wang, *Appl. Energy*, 2015, **159**, 502–508.
- 53 L. T. Kang, Y. F. Gao, Z. T. Zhang, J. Du, C. X. Cao, Z. Chen and H. J. Luo, *J. Phys. Chem. C*, 2010, **114**, 1901–1911.
- 54 M. R. Bayati, R. Molaei, F. Wu, J. D. Budai, Y. Liu, R. J. Narayan and J. Narayan, *Acta Mater.*, 2013, **61**, 7805–7815.
- 55 J. Jian, A. Chen, Y. Chen, X. Zhang and H. Wang, *Appl. Phys. Lett.*, 2017, **111**, 153102.
- 56 B. Zhi, G. Gao, X. Tan, P. Chen, L. Wang, S. Jin and W. Wu, *Mater. Res. Express*, 2014, **1**, 046402.
- 57 R. Molaei, R. Bayati, F. Wu and J. Narayan, *J. Appl. Phys.*, 2014, **115**, 164311.
- 58 J. Lappalainen, S. Heinilehto, S. Saukko, W. Lantto and H. Jantunen, *Sens. Actuators, A*, 2008, **142**, 250–255.
- 59 Z. P. Wu, *Defects and Diffusion in Ceramics*, 2000, **186**, 137–143.
- 60 H. Koo, S. Yoon, O. J. Kwon, K.-E. Ko, D. Shin, S.-H. Bae, S.-H. Chang and C. Park, *J. Mater. Sci.*, 2012, **47**, 6397–6401.
- 61 K. Shibuya, J. y. Tsutsumi, T. Hasegawa and A. Sawa, *Appl. Phys. Lett.*, 2013, **103**, 021604.
- 62 K. Shibuya and A. Sawa, *Jpn. J. Appl. Phys.*, 2014, **53**, 05FF03.
- 63 Y. Muraoka, Y. Ueda and Z. Hiroi, *J. Phys. Chem. Solids*, 2002, **63**, 965–967.
- 64 K. Nagashima, T. Yanagida, H. Tanaka and T. Kawai, *J. Appl. Phys.*, 2006, **100**, 063714.
- 65 K. Nagashima, T. Yanagida, H. Tanaka and T. Kawai, *J. Appl. Phys.*, 2007, **101**, 026103.
- 66 J. Li and J. Dho, *J. Cryst. Growth.*, 2014, **404**, 84–88.
- 67 J. A. Li and J. Dho, *J. Cryst. Growth.*, 2010, **312**, 3287–3291.

- 68 E. Breckenfeld, H. Kim, K. Burgess, N. Charipar, S.-F. Cheng, R. Stroud and A. Pique, *ACS Appl. Mater. Interfaces*, 2017, **9**, 1577–1584.
- 69 T. Slusar, J.-C. Cho, B.-J. Kim, S. J. Yun and H.-T. Kim, *APL Mater.*, 2016, **4**, 026101.
- 70 H. Kim, N. S. Bingham, N. A. Charipar and A. Pique, *AIP Adv.*, 2017, **7**, 105116.
- 71 T.-H. Yang, S. Mal, C. Jin, R. J. Narayan and J. Narayan, *Appl. Phys. Lett.*, 2011, **98**, 022105.
- 72 R. Molaei, M. R. Bayati and J. Narayan, *J. Mater. Res.*, 2012, **27**, 3103–3109.
- 73 J. Narayan and B. C. Larson, *J. Appl. Phys.*, 2003, **93**, 278–285.
- 74 K. Martens, N. Aetukuri, J. Jeong, M. G. Samant and S. S. P. Parkin, *Appl. Phys. Lett.*, 2014, **104**, 081918.
- 75 L. L. Fan, S. Chen, Y. F. Wu, F. H. Chen, W. S. Chu, X. Chen, C. W. Zou and Z. Y. Wu, *Appl. Phys. Lett.*, 2013, **103**, 131914.
- 76 Y. F. Gao, S. B. Wang, H. J. Luo, L. Dai, C. X. Cao, Y. L. Liu, Z. Chen and M. Kanehira, *Energy Environ. Sci.*, 2012, **5**, 6104–6110.
- 77 Z. Chen, Y. F. Gao, L. T. Kang, C. X. Cao, S. Chen and H. J. Luo, *J. Mater. Chem. A*, 2014, **2**, 2718–2727.
- 78 Z. Chen, C. X. Cao, H. J. Luo and Y. F. Gao, *Chin. Sci. Bull.*, 2016, **61**, 18.
- 79 L. A. Gea, L. A. Boatner, H. M. Evans and R. Zuhr, *Nucl. Instrum. Methods Phys. Res., Sect. B*, 1997, **127**, 553–556.
- 80 R. Lopez, L. A. Boatner, T. E. Haynes, R. F. Haglund and L. C. Feldman, *Appl. Phys. Lett.*, 2001, **79**, 3161–3163.
- 81 H. Karl, J. Dreher and B. Stritzker, in *Functional Metal-Oxide Nanostructures*, ed. J. Wu, W. Q. Han, A. Janotti and H. C. Kim, 2009, vol. 1174, pp. 107–112.
- 82 L. A. Gea and L. A. Boatner, *Appl. Phys. Lett.*, 1996, **68**, 3081–3083.
- 83 A. Meldrum, R. Lopez, R. H. Magruder, L. A. Boatner and C. W. White, in *Materials Science with Ion Beams*, ed. H. Bernas, Springer-Verlag Berlin, Berlin, 2010, vol. 116, pp. 255–285.
- 84 H. Lim, N. Stavrias, B. C. Johnson, R. E. Marvel, R. F. Haglund and J. C. McCallum, *J. Appl. Phys.*, 2014, **115**, 093107.
- 85 P. Jin, S. Nakao and S. Tanemura, *Thin Solid Films*, 1998, **324**, 151–158.
- 86 T. Jostmeier, J. Zimmer, H. Karl, H. J. Krenner and M. Betz, *Appl. Phys. Lett.*, 2014, **105**, 4.
- 87 R. Lopez, L. C. Feldman and R. F. Haglund, *Phys. Rev. Lett.*, 2004, **93**, 177403.
- 88 R. Lopez, T. E. Haynes, L. A. Boatner, L. C. Feldman and R. F. Haglund, *Phys. Rev. B: Condens. Matter Mater. Phys.*, 2002, **65**, 224113.
- 89 E. U. Donev, R. Lopez, L. C. Feldman and R. F. Haglund, *Nano Lett.*, 2009, **9**, 702–706.
- 90 M. Rini, A. Cavalleri, R. W. Schoenlein, R. Lopez, L. C. Feldman, R. F. Haglund, L. A. Boatner and T. E. Haynes, *Opt. Lett.*, 2005, **30**, 558–560.
- 91 T. Jostmeier, M. Mangold, J. Zimmer, H. Karl, H. J. Krenner, C. Ruppert and M. Betz, *Opt. Express*, 2016, **24**, 17321–17331.
- 92 Y. Zhou, A. Huang, Y. Li, S. Ji, Y. Gao and P. Jin, *Nanoscale*, 2013, **5**, 9208–9213.
- 93 S. J. Jiang, C. B. Ye, M. S. Khan and C. G. Granqvist, *Appl. Opt.*, 1991, **30**, 847–851.
- 94 G. Golan, A. Axelevitch, B. Sigalov and B. Gorenstein, *Microelectron. J.*, 2003, **34**, 255–258.
- 95 M. A. Manthrammel, A. Fatehmulla, A. M. Al-Dhafiri, A. S. Alshammari and A. Khan, *Opt. Spectrosc.*, 2017, **122**, 420–425.
- 96 A. Paone, R. Sanjines, P. Jeanneret, H. J. Whitlow, E. Guibert, G. Guibert, F. Bussy, J.-L. Scartezzini and A. Schueler, *J. Alloys Compd.*, 2015, **621**, 206–211.
- 97 J.-S. Ke, S.-F. Weng, M.-C. Wu and C.-S. Lee, *J. Nanopart. Res.*, 2013, **15**, 1632.
- 98 A. Axelevitch, B. Gorenstein and G. Golan, *Microelectron. Reliab.*, 2011, **51**, 2119–2123.
- 99 Q. Guo, S. Lee and D. W. Goodman, *Surf. Sci.*, 1999, **437**, 38–48.
- 100 L. Ortega-Reyes and A. Avila-Garcia, *Mater. Sci. Semicond. Process.*, 2015, **37**, 123–128.
- 101 R. E. Marvel, K. Appavoo, B. K. Choi, J. Nag and R. F. Haglund, *Appl. Phys. A: Mater. Sci. Process.*, 2013, **111**, 975–981.
- 102 A. Crunteanu, M. Fabert, J. Cornette, M. Colas, J.-C. Orlianges, A. Bessaoudou and F. Cosset, in *Oxide-Based Materials and Devices VI*, ed. F. H. Teherani, D. C. Look and D. J. Rogers, 2015, vol. 9364.
- 103 J. Leroy, A. Bessaoudou, F. Cosset and A. Crunteanu, *Thin Solid Films*, 2012, **520**, 4823–4825.
- 104 V. Thery, A. Boulle, A. Crunteanu, J. C. Orlianges, A. Beaumont, R. Mayet, A. Mennai, F. Cosset, A. Bessaoudou and M. Fabert, *Phys. Rev. B: Condens. Matter Mater. Phys.*, 2016, **93**, 184106.
- 105 V. Thery, A. Boulle, A. Crunteanu, J. C. Orlianges, A. Beaumont, R. Mayet, A. Mennai, F. Cosset, A. Bessaoudou and M. Fabert, *J. Appl. Phys.*, 2017, **121**, 055303.
- 106 M. H. Lee, M. G. Kim and H. K. Song, *Thin Solid Films*, 1996, **290**, 30–33.
- 107 R. E. Marvel, R. R. Harl, V. Craciun, B. R. Rogers and R. F. Haglund, Jr., *Acta Mater.*, 2015, **91**, 217–226.
- 108 P. Jin, G. Xu, M. Tazawa and K. Yoshimura, *Jpn. J. Appl. Phys.*, 2002, **41**(2), L278–L280.
- 109 M. Sambi, M. Della Negra, G. Granozzi, Z. S. Li, J. H. Jorgensen and P. J. Moller, *Appl. Surf. Sci.*, 1999, **142**, 146–151.
- 110 M. Sambi, G. Sangiovanni, G. Granozzi and F. Parmigiani, *Phys. Rev. B: Condens. Matter Mater. Phys.*, 1997, **55**, 7850–7858.
- 111 J. W. Tashman, J. H. Lee, H. Paik, J. A. Moyer, R. Misra, J. A. Mundy, T. Spila, T. A. Merz, J. Schubert, D. A. Muller, P. Schiffer and D. G. Schlom, *Appl. Phys. Lett.*, 2014, **104**, 5.
- 112 H. Paik, J. A. Moyer, T. Spila, J. W. Tashman, J. A. Mundy, E. Freeman, N. Shukla, J. M. Lapano, R. Engel-Herbert, W. Zander, J. Schubert, D. A. Muller, S. Datta, P. Schiffer and D. G. Schlom, *Appl. Phys. Lett.*, 2015, **107**, 163101.
- 113 L. L. Fan, S. Chen, Z. L. Luo, Q. H. Liu, Y. F. Wu, L. Song, D. X. Ji, P. Wang, W. S. Chu, C. Gao, C. W. Zou and Z. Y. Wu, *Nano Lett.*, 2014, **14**, 4036–4043.
- 114 L. L. Fan, S. Chen, Q. H. Liu, G. M. Liao, Y. L. Chen, H. Ren and C. W. Zou, *J. Alloys Compd.*, 2016, **678**, 312–316.
- 115 Y. C. Lin, K. DeLello, H. T. Zhang, K. H. Zhang, Z. Lin, M. Terrones, R. Engel-Herbert and J. A. Robinson, *J. Phys.: Condens. Matter*, 2016, **28**, 7.

- 116 L. L. Fan, Y. L. Chen, Q. H. Liu, S. Chen, L. Zhu, Q. Q. Meng, B. L. Wang, Q. F. Zhang, H. Ren and C. W. Zou, *ACS Appl. Mater. Interfaces*, 2016, **8**, 32971–32977.
- 117 Y.-B. Kang, *J. Eur. Ceram. Soc.*, 2012, **32**, 3187–3198.
- 118 C. H. Griffiths and H. K. Eastwood, *J. Appl. Phys.*, 1974, **45**, 2201–2206.
- 119 H. Yuce, H. Alaboz, Y. Demirhan, M. Ozdemir, L. Ozyuzer and G. Aygun, *Phys. Scr.*, 2017, **92**, 114007.
- 120 Y. Zhao, C. Chen, X. Pan, Y. Zhu, M. Holtz, A. Bernussi and Z. Fan, *J. Appl. Phys.*, 2013, **114**, 113509.
- 121 B. Zhu, H. Tao and X. Zhao, *Infrared Phys. Technol.*, 2016, **75**, 22–25.
- 122 M. Zhu, H. Qi, B. Wang, H. Wang, T. Guan and D. Zhang, *J. Alloys Compd.*, 2018, **740**, 844–851.
- 123 Q. Yu, W. Li, J. Liang, Z. Duan, Z. Hu, J. Liu, H. Chen and J. Chu, *J. Phys. D: Appl. Phys.*, 2013, **46**, 055310.
- 124 Y.-K. Dou, J.-B. Li, M.-S. Cao, D.-Z. Su, F. Rehman, J.-S. Zhang and H.-B. Jin, *Appl. Surf. Sci.*, 2015, **345**, 232–237.
- 125 Z. Huang, S. Chen, C. Lv, Y. Huang and J. Lai, *Appl. Phys. Lett.*, 2012, **101**, 191905.
- 126 H. Y. Xu, Y. H. Huang, J. P. Li, F. Ma and K. W. Xu, *J. Vac. Sci. Technol., A*, 2015, **33**, 061508.
- 127 G. Sun, H. Zhou, X. Cao, R. Li, M. Tazawa, M. Okada and P. Jin, *ACS Appl. Mater. Interfaces*, 2016, **8**, 7054–7059.
- 128 G. Sun, X. Cao, Y. Yue, X. Gao, S. Long, N. Li, R. Li, H. Luo and P. Jin, *Sci. Rep.*, 2018, **8**, 5342.
- 129 Z. Chen, X. Wang, Y. Qi, S. Yang, J. A. Soares, B. A. Apgar, R. Gao, R. Xu, Y. Lee, X. Zhang, J. Yao and L. W. Martin, *ACS Nano*, 2016, **10**, 10237–10244.
- 130 H. Kakiuchida, P. Jin and M. Tazawa, *Int. J. Thermophys.*, 2009, **31**, 1964–1971.
- 131 S. Loquai, B. Baloukas, J. E. Klemburg-Sapieha and L. Martinu, *Sol. Energy Mater. Sol. Cells*, 2017, **160**, 217–224.
- 132 T. Ben-Messaoud, G. Landry, J. P. Gariépy, B. Ramamoorthy, P. V. Ashrit and A. Haché, *Opt. Commun.*, 2008, **281**, 6024–6027.
- 133 M. Jiang, X. Cao, S. Bao, H. Zhou and P. Jin, *Thin Solid Films*, 2014, **562**, 314–318.
- 134 M. Jiang, Y. Li, S. Li, H. Zhou, X. Cao, S. Bao, Y. Gao, H. Luo and P. Jin, *J. Nanomater.*, 2014, **2014**, 1–6.
- 135 M. Panagopoulou, E. Gagaoudakis, E. Aperathitis, I. Michail, G. Kiriakidis, D. Tsoukalas and Y. S. Raptis, *Thin Solid Films*, 2015, **594**, 310–315.
- 136 N. H. Azhan, K. Okimura, Y. Ohtsubo, S.-i. Kimura, M. Zaghrioui and J. Sakai, *J. Appl. Phys.*, 2016, **119**, 055308.
- 137 N. H. Azhan, K. Su, K. Okimura and J. Sakai, *J. Appl. Phys.*, 2015, **117**, 185307.
- 138 A. Ajaz, Y.-X. Ji, J. Montero, G. A. Niklasson, C. G. Granqvist and T. Kubart, *Sol. Energy Mater. Sol. Cells*, 2016, **149**, 137–144.
- 139 S. Loquai, B. Baloukas, O. Zabeida, J. E. Klemburg-Sapieha and L. Martinu, *Sol. Energy Mater. Sol. Cells*, 2016, **155**, 60–69.
- 140 J. P. Fortier, B. Baloukas, O. Zabeida, J. E. Klemburg-Sapieha and L. Martinu, *Sol. Energy Mater. Sol. Cells*, 2014, **125**, 291–296.
- 141 J. Houska, D. Kolenaty, J. Rezek and J. Vlcek, *Appl. Surf. Sci.*, 2017, **421**, 529–534.
- 142 M. S. Mian and K. Okimura, *Jpn. J. Appl. Phys.*, 2014, **53**, 035802.
- 143 M. S. Mian and K. Okimura, *J. Vac. Sci. Technol., A*, 2014, **32**, 041502.
- 144 T. Nakamura and K. Okimura, *Vacuum*, 2004, **74**, 391–395.
- 145 Y. Nihei, Y. Sasakawa and K. Okimura, *Thin Solid Films*, 2008, **516**, 3572–3576.
- 146 T. Watanabe, K. Okimura, T. Hajiri, S.-i. Kimura and J. Sakai, *J. Appl. Phys.*, 2013, **113**, 163503.
- 147 J. B. K. Kana, J. M. Ndjaka, P. O. Ateba, B. D. Ngom, N. Manyala, O. Nemraoui, A. C. Beye and M. Maaza, *Appl. Surf. Sci.*, 2008, **254**, 3959–3963.
- 148 J. B. Kana Kana, J. M. Ndjaka, B. D. Ngom, A. Y. Fasasi, O. Nemraoui, R. Nemutudi, D. Knoesen and M. Maaza, *Opt. Mater.*, 2010, **32**, 739–742.
- 149 C. O. F. Ba, S. T. Bah, M. D'Auteuil, V. Fortin, P. V. Ashrit and R. Vallée, *Curr. Appl. Phys.*, 2014, **14**, 1531–1537.
- 150 X. Yi, C. Chen, L. Liu, Y. Wang, B. Xiong, H. Wang and S. Chen, *Infrared Phys. Technol.*, 2003, **44**, 137–141.
- 151 J. Liang, M. Hu, Q. Kan, X. Liang, X. Wang, G. Li and H. Chen, *Rare Met.*, 2011, **30**, 247–251.
- 152 J. H. Yu, S. H. Nam, J. W. Lee and J. H. Boo, *Materials*, 2016, **9**, 556.
- 153 G. Sun, X. Cao, X. Li, S. Bao, N. Li, M. Liang, A. Gloter, H. Gu and P. Jin, *Sol. Energy Mater. Sol. Cells*, 2017, **161**, 70–76.
- 154 M. I. Kang, I. K. Kim, E. J. Oh, S. W. Kim, J. W. Ryu and H. Y. Park, *Thin Solid Films*, 2012, **520**, 2368–2371.
- 155 X. Chu, H. Tao, M. Wan, S. Wang, Z. Ning, N. Xu and X. Zhao, *J. Wuhan Univ. Technol., Mater. Sci. Ed.*, 2014, **29**, 1117–1123.
- 156 J.-R. Liang, M.-J. Wu, M. Hu, J. Liu, N.-W. Zhu, X.-X. Xia and H.-D. Chen, *Chin. Phys. B*, 2014, **23**, 076801.
- 157 X. Liu, S.-W. Wang, F. Chen, L. Yu and X. Chen, *J. Phys. D: Appl. Phys.*, 2015, **48**, 265104.
- 158 Z. Luo, Z. Wu, X. Xu, T. Wang and Y. Jiang, *J. Vac. Sci. Technol., A*, 2010, **28**, 595–599.
- 159 H. Xiao, Y. Li, W. Yuan, B. Fang, X. Wang, R. Hao, Z. Wu, T. Xu, W. Jiang and P. Chen, *Infrared Phys. Technol.*, 2016, **76**, 580–586.
- 160 N.-W. Zhu, M. Hu, X.-X. Xia, X.-Y. Wei and J.-R. Liang, *Chin. Phys. B*, 2014, **23**, 048108.
- 161 N. Wang, S. Liu, X. T. Zeng, S. Magdassi and Y. Long, *J. Mater. Chem. C*, 2015, **3**, 6771–6777.
- 162 X.-J. Wang, Y.-Y. Liu, D.-H. Li, B.-H. Feng, Z.-W. He and Z. Qi, *Chin. Phys. B*, 2013, **22**, 066803.
- 163 M. D. Zhu, D. P. Zhang, Y. Liu, K. Yang, G. X. Liang, Z. H. Zheng and P. Fan, *Mater. Sci. Forum*, 2016, **847**, 184–189.
- 164 C. Ji, Z. Wu, X. Wu, J. Wang, J. Gou, Z. Huang, H. Zhou, W. Yao and Y. Jiang, *Sol. Energy Mater. Sol. Cells*, 2018, **176**, 174–180.
- 165 E. Gagaoudakis, I. Kortidis, G. Michail, K. Tsagaraki, V. Binias, G. Kiriakidis and E. Aperathitis, *Thin Solid Films*, 2016, **601**, 99–105.
- 166 S.-Y. Li, G. A. Niklasson and C. G. Granqvist, *J. Appl. Phys.*, 2014, **115**, 053513.

- 167 M. Panagopoulou, E. Gagaoudakis, N. Boukos, E. Aperathitis, G. Kiriakidis, D. Tsoukalas and Y. S. Raptis, *Sol. Energy Mater. Sol. Cells*, 2016, **157**, 1004–1010.
- 168 X. Wu, Z. Wu, H. Zhang, R. Niu, Q. He, C. Ji, J. Wang and Y. Jiang, *Surf. Coat. Technol.*, 2015, **276**, 248–253.
- 169 H. Zhang, Z. Wu, R. Niu, X. Wu, Q. He and Y. Jiang, *Appl. Surf. Sci.*, 2015, **331**, 92–97.
- 170 H. Zhou, X. Cao, M. Jiang, S. Bao and P. Jin, *Laser Photonics Rev.*, 2014, **8**, 617–625.
- 171 G. Xu, C.-M. Huang, M. Tazawa, P. Jin and L.-H. Chen, *Opt. Commun.*, 2009, **282**, 896–902.
- 172 G. Xu, Y. Chen, M. Tazawa and P. Jin, *J. Phys. Chem. B*, 2006, **110**, 2051–2056.
- 173 G. Xu, C.-M. Huang, M. Tazawa, P. Jin and D.-M. Chen, *J. Appl. Phys.*, 2008, **104**, 053101.
- 174 G. Xu, C.-M. Huang, P. Jin, M. Tazawa and D.-M. Chen, *J. Appl. Phys.*, 2008, **104**, 053102.
- 175 H. Koo, H. You, K.-E. Ko, O. J. Kwon, S.-H. Chang and C. Park, *Appl. Surf. Sci.*, 2013, **277**, 237–241.
- 176 H. Koo, L. Xu, K.-E. Ko, S. Ahn, S.-H. Chang and C. Park, *J. Mater. Eng. Perform.*, 2013, **22**, 3967–3973.
- 177 G. Sun, X. Cao, X. Gao, S. Long, M. Liang and P. Jin, *Appl. Phys. Lett.*, 2016, **109**, 143903.
- 178 S. Long, X. Cao, G. Sun, N. Li, T. Chang, Z. Shao and P. Jin, *Appl. Surf. Sci.*, 2018, **441**, 764–772.
- 179 J. Montero, Y.-X. Ji, S.-Y. Li, G. A. Niklasson and C. G. Granqvist, *J. Vac. Sci. Technol., B: Nanotechnol. Microelectron.: Mater., Process., Meas., Phenom.*, 2015, **33**, 031805.
- 180 T. Chang, X. Cao, N. Li, S. Long, X. Gao, L. R. Dedon, G. Sun, H. Luo and P. Jin, *ACS Appl. Mater. Interfaces*, 2017, **9**, 26029–26037.
- 181 T. Chang, X. Cao, L. R. Dedon, S. Long, A. Huang, Z. Shao, N. Li, H. Luo and P. Jin, *Nano Energy*, 2018, **44**, 256–264.
- 182 G. Xu, P. Jin, M. Tazawa and K. Yoshimura, *Sol. Energy Mater. Sol. Cells*, 2004, **83**, 29–37.
- 183 Y.-X. Ji, S.-Y. Li, G. A. Niklasson and C. G. Granqvist, *Thin Solid Films*, 2014, **562**, 568–573.
- 184 J. Zheng, S. Bao and P. Jin, *Nano Energy*, 2015, **11**, 136–145.
- 185 N. R. Mlyuka, G. A. Niklasson and C. G. Granqvist, *Sol. Energy Mater. Sol. Cells*, 2009, **93**, 1685–1687.
- 186 G. Sun, X. Cao, H. Zhou, S. Bao and P. Jin, *Sol. Energy Mater. Sol. Cells*, 2017, **159**, 553–559.
- 187 M. Tazawa, K. Yoshimura, P. Jin and G. Xu, *Appl. Phys. A: Mater. Sci. Process.*, 2003, **77**, 455–459.
- 188 S. Long, X. Cao, N. Li, Y. Xin, G. Sun, T. Chang, S. Bao and P. Jin, *Sol. Energy Mater. Sol. Cells*, 2019, **189**, 138–148.
- 189 S. Long, H. Zhou, S. Bao, Y. Xin, X. Cao and P. Jin, *RSC Adv.*, 2016, **6**, 106435–106442.
- 190 C. Zhang, C. ChuanXiang, L. HongJie and G. YanFeng, *Chin. Sci. Bull.*, 2016, **61**, 1661.
- 191 Y. Ke, X. Wen, D. Zhao, R. Che, Q. Xiong and Y. Long, *ACS Nano*, 2017, **11**, 7542–7551.
- 192 X. Cao, N. Wang, J. Y. Law, S. C. J. Loo, S. Magdassi and Y. Long, *Langmuir*, 2014, **30**, 1710–1715.
- 193 J. Y. Zheng, S. H. Bao and P. Jin, *Nano Energy*, 2015, **11**, 136–145.
- 194 J. D. Zhou, Y. F. Gao, Z. T. Zhang, H. J. Luo, C. X. Cao, Z. Chen, L. Dai and X. L. Liu, *Sci. Rep.*, 2013, **3**, 3029.
- 195 F. Guo, S. Chen, Z. Chen, H. Luo, Y. Gao, T. Przybilla, E. Spiecker, A. Osset, K. Forberich and C. J. Brabec, *Adv. Opt. Mater.*, 2015, **3**, 1524–1529.
- 196 Z. Chen, C. Cao, S. Chen, H. Luo and Y. Gao, *J. Mater. Chem. A*, 2014, **2**, 11874–11884.
- 197 F. Yang, X. Shi, Z. Chen, D. Ma, Y. Wu, H. Luo and Y. Gao, *RSC Adv.*, 2016, **6**, 32176–32182.